Fluctuation spectrum and transport from ion temperature gradient driven modes in sheared magnetic fields

Cite as: Physics of Fluids B: Plasma Physics **2**, 1833 (1990); https://doi.org/10.1063/1.859455
Submitted: 13 September 1989 . Accepted: 05 April 1990 . Published Online: 04 June 1998

Satoshi Hamaguchi, and Wendell Horton

Fluctuation spectrum and transport from ion temperature gradient driven modes in sheared magnetic fields

Satoshi Hamaguchi and Wendell Horton
Institute for Fusion Studies, The University of Texas at Austin, Austin, Texas 78712

(Received 13 September 1989; accepted 5 April 1990)

The ion temperature gradient driven mode or η_i-mode turbulence is reinvestigated based on two-component compressible fluid equations with the polarization drift velocity and adiabatic electrons. The scaling of the anomalous ion heat conductivity with magnetic shear $s = L_n/L_s$ and the excess of η_i over the critical value $\eta_{i,c}$ for marginal stability is found to vary as $\chi_i = g(\rho_s/L_n)(cT_i/eB)(\eta_i - \eta_{i,c})\exp(-\alpha s)$, where $g \simeq 1$ and $\alpha \simeq 5$.

I. INTRODUCTION

Recent experimental studies in tokamaks both with regard to the ion thermal confinement properties[1-3] and with respect to the fluctuation spectrum[4] indicate that the ion temperature gradient driven drift mode or η_i mode[5,6] is probably a determining part of the thermal confinement properties in tokamaks. In view of these experimental developments we reconsider some of the theoretical differences[7-10] that are found in the earlier formulas for the η_i-mode turbulence and the associated anomalous ion heat conductivity χ_i. In particular we investigate the magnetic shear $s = L_n/L_s$ dependence of the anomalous heat conductivity $\chi_i(s)$. Here L_n and L_s denote the scale lengths of the density gradient and the magnetic shear, respectively. The early 3-D nonlinear study of Horton, Estes, and Biskamp[7] reports that χ_i decreases weakly as $s^{-1/2}$ with increasing shear, whereas the subsequent theoretical works of Connor,[8] and Lee and Diamond[9] indicate the opposite tendency with χ_i increasing linearly with the shear s. Recent work of Terry *et al.*[10] argues that the anomalous ion heat conductivity χ_i obtained by Lee and Diamond[9] should be enhanced by the factor $(2l+1)^2$ from the effect of unstable radial eigenmode numbers l. In the work of Connor,[8] such scaling of χ_i was derived using dimensional analysis of a system further simplified from the original sheared slab model of the η_i mode. In the work of Lee and Diamond[9] and the work of Terry *et al.*[10] the authors essentially attempt to explain the shear dependence of χ_i with the linear growth rate increasing linearly with the shear s under the assumption of small poloidal mode numbers [$k_y^2\rho^2(\eta_i+1) \ll 1$ with k_y being the poloidal wave number, ρ being the ion Larmor radius, $\eta_i = L_n/L_T$, and L_T being the scale length of the ion temperature gradient] and fixed radial eigenmode numbers l. The dependence of χ_i on the ion temperature gradient η_i is also of basic importance. In these previous works the η_i dependence of χ_i scales as $\chi_i \propto (\eta_i+1)^\alpha$ with $\frac{1}{2} \lesssim \alpha \lesssim 2$. Since the model equations of the η_i mode on which all these previous results are based are the same,[11] the correct scaling of the ion anomalous heat transport χ_i due to the slab η_i-mode turbulence has not been established yet.

In order to settle this discrepancy, we reinvestigate the problem using more rigorous analyses and numerical simulations based on the same two-component compressible fluid equations with adiabatic electrons. The parameter regime of interest is $s \ll 1$ and finite L_n, a typical parameter regime of high-temperature tokamak plasmas. We solve the linear eigenvalue problem analytically with perturbation theory and numerically with the shooting code and the initial-value code. Based on the space-time scale obtained from the linear analysis, mixing length theory is applied to estimate the anomalous ion heat conductivity, which is then compared to the results of the amplitude expansion method and numerical simulations. In the amplitude expansion method, the set of nonlinear equations of the η_i mode is solved rigorously near the marginally stable state, and the dependence of χ_i on the ion temperature gradient η_i is obtained. The nonlinear initial-value code is used to solve the 2-D and 3-D equations for finite amplitude fluctuations. In the steady state of turbulence the scaling of the anomalous ion heat conductivity $\chi_i(s,\eta_i)$ is obtained for a wide range of the parameter space. The simulations use a second-order finite difference formula in the radial direction x and Fourier component representations in the perpendicular y and z directions. This numerical method contrasts with the finite difference formulas in the three-space directions with upwind derivatives in the $\mathbf{E}\times\mathbf{B}\cdot\nabla$ nonlinearity used by Horton, Estes, and Biskamp.[7]

An important result of the stability analysis is that the linear mode is most strongly excited when $k_y\rho_s \simeq (1+\eta_i)^{-1/2}$ and $(2l+1)s \simeq$ const and the growth rate of this fastest growing mode γ_m is a weakly decreasing function of shear while localization of the mode around the mode rational surface becomes stronger with increasing shear. Suppose such strongly excited linear modes are responsible for the nonlinearly saturated turbulent state, the associated anomalous ion heat transport can be shown to decrease with increasing shear, unlike the χ_i scalings reported in Refs. 8 and 9. Although numerical simulations show that the peak of energy spectrum is downshifted from the wave number giving the fastest growing linear mode, the mixing length estimate based on the most unstable linear mode provides the general tendency of the χ_i scaling that agrees reasonably well with the numerical results. Physically, this is expected since the fastest growing linear mode is the energy input to the turbulence.

Based on a more rigorous nonlinear analysis and parametrization of the numerical results, we find that the anomalous ion heat conductivity is given by

$$\chi_i = g(\rho_s/L_n)(cT_i/eB)(\eta_i - \eta_{i,c})\exp(-\alpha s), \quad (1)$$

 0899-8221/90/081833-19$02.00

when η_i is close to its critical value $\eta_{i,c}$ ($\eta_{i,c} \lesssim \eta_i \lesssim 3$). Here $g \simeq 1$ and $\alpha \simeq 5$. We note that although the parameter $\alpha = \alpha(\eta_i)$ in Eq. (1) is generally a function of η_i, we use $\alpha = \alpha(\eta_{i,c}) \simeq 5$ here. In the limit of $\eta_i \to \infty$, however, Eq. (1) is transformed to the following formula obtained from numerical simulations:

$$\chi_i = g\frac{\rho_s}{L_T}\left(\frac{cT_i}{eB}\right)\exp\left(-\beta\frac{T_e}{T_i}\frac{L_T}{L_s}\right),$$

where $\beta \simeq 4$. In other words, $\alpha(\eta_i) \to (T_e/T_i)(\beta/\eta_i)$ as $\eta_i \to \infty$. The detailed study of the dependence of α on general η_i will be presented in the future.

In deriving the shear dependence $\chi_i(s)$ in Eq. (1), we consider both power law s^ν and exponential fits. With the alternative power law parametrization of $\chi_i(s)$ we obtain $\nu = -2$ for $s \gtrsim 0.5$, as in resistive g-mode turbulence, and $\nu = -\frac{1}{2}$ for $s \simeq 0.1$. As shown in Sec. V, the exponential dependence fits well the entire range of shear. It is found that the scaling obtained by Horton, Estes, and Biskamp[7] agrees reasonably well with the scaling above in the limited range of the shear parameter $0.05 \lesssim s \lesssim 0.1$ while it underestimates the strength of the shear dependence for larger shear. On the other hand, the scalings of Connor,[8] and Lee and Diamond[9] ($\nu = 1$) give wrong qualitative dependence on shear; i.e., χ_i increasing with shear.

For smaller shear, the locally unfavorable toroidal curvature $\epsilon_n = L_n/R$ effects are dominant[12-16] and the sheared slab model of the η_i mode becomes no longer applicable. The anomalous ion heat conductivity χ_i calculated by Horton, Choi, and Tang[12] from the toroidal η_i mode, however, also shows that χ_i is a decreasing function of shear, scaling as $\chi_i \propto 1/s$. In the work of Hong and Horton,[17] the limit $s \to 0$ of the toroidal η_i mode is reexamined. For sufficiently small shear, the radial profile of the electron diamagnetic frequency $\omega_*(r)$ and the ion temperature gradient $\eta_i(r)$ must be taken into account over the mode width Δr.

The present work is organized as follows. In Sec. II we give the nondimensional field variables and the dynamical equations along with their conservation properties. In Sec. III the linear analysis is presented, assessing the shear stabilization effect due to the parallel compressibility and the parallel diffusion. In Sec. III we also present the mixing length estimate, deriving as a reference formula the anomalous ion heat conductivity $\chi_i(s,\eta_i)$ of the η_i-mode turbulence. In Sec. IV, the amplitude expansion method is used to solve the nonlinear equations and the η_i dependence of χ_i is obtained. The results of the 2-D and 3-D numerical simulations are shown in Sec. V and the scaling of χ_i is derived therein. The conclusions and brief critiques to the previous results are given in Sec. VI.

II. DYNAMICAL EQUATIONS

In this section we present the dynamical equations of the ion temperature gradient driven mode and review their basic properties. The fluid model of the electrostatic ion temperature gradient driven mode in a sheared slab is derived[7] from the two-component fluid equations (Braginskii equations)[18] with the finite ion Larmor radius stress tensor and the ion heat balance equation. Assuming charge neutrality, constant electron temperature, and zero electron inertia, the parallel component of the electron momentum balance equations is used to derive a Boltzman distribution of electrons

$$n = n_i = n_e = n_0(x)(1 + e\Phi/T_e), \tag{2}$$

where n_i and n_e are the ion and electron densities, respectively, $n_0(x)$ is the unperturbed density, $\Phi = \Phi(x,y,z,t)$ is the electric potential, $e (e > 0)$ is the magnitude of the electron charge, and T_e is the (constant) electron temperature. In Eq. (2) we assumed that $|e\Phi/T_e| \ll 1$. The coordinate system (x,y,z) is the usual orthogonal coordinate system represented by three unit vectors $\hat{\mathbf{x}}$, $\hat{\mathbf{y}}$, and $\hat{\mathbf{z}}$. Here $\hat{\mathbf{x}}$ represents the radial direction of a plasma cylinder, $\hat{\mathbf{z}}$ represents the direction of the magnetic field $\mathbf{B}$ at a rational surface, the position of which is indicated by $x = x_0$. To the lowest order, the ion fluid velocity $\mathbf{v}$ may be written as the sum of the $\mathbf{E}\times\mathbf{B}$ drift velocity $\mathbf{v}_E$ and the ion diamagnetic drift velocity $\mathbf{v}_D$, where

$$\mathbf{v}_E = c[(\mathbf{E}\times\mathbf{B})/B^2]$$

and

$$\mathbf{v}_D = c[(\hat{\mathbf{z}}\times\nabla p_i)/enB].$$

Here $\mathbf{E} = -\nabla\Phi$ is the electric field, c is the light velocity, $B = |\mathbf{B}|$ is the magnitude of the magnetic field at $x = x_0$, and p_i is the ion pressure. To the next order of $\mathbf{v}$, we have the polarization drift velocity

$$\mathbf{v}_p = \frac{-c^2 m_i}{eB^2}\left(\frac{\partial}{\partial t} + (\mathbf{v}_E + \mathbf{v}_D)\cdot\nabla\right)\nabla_\perp\Phi, \tag{3}$$

where m_i is the ion mass and $\nabla_\perp$ is the gradient perpendicular to the direction of the magnetic field $\mathbf{B}$. Denoting the parallel velocity by $v_\parallel$, we write

$$n = n_0(x) + \tilde{n} = n_0 + n_0 e\Phi/T_e,$$

$$p_i = p_{i0}(x) + \tilde{p}_i,$$

$$\Phi = \tilde{\Phi}, \text{ and } v_\parallel = \tilde{v}_\parallel,$$

where the subscript 0 denotes the unperturbed quantities which are assumed to be functions of only x, and the tilde denotes the fluctuating quantities. Here we assume that the unperturbed parts of the velocity field $\mathbf{v}$ and the potential Φ are zero. In order to write down the dynamical equations in a nondimensional form, we define the following characteristic velocity and space scales:

$$c_s = \left(\frac{T_e}{m_i}\right)^{1/2}, \quad \rho_s = \frac{c_s}{\omega_{ci}} = \frac{c(m_i T_e)^{1/2}}{eB},$$

$$L_n = -\left(\frac{d}{dx}\ln n_0\right)^{-1}, \quad L_T = -\left(\frac{d}{dx}\ln T_{i0}\right)^{-1},$$

and the nondimensional parameters

$$\eta_i = L_n/L_T, \quad K = (T_i/T_e)(1 + \eta_i), \quad \Gamma = \gamma T_i/T_e. \tag{4}$$

Here γ denotes the ratio of the specific heats, ω_{ci} is the ion cyclotron frequency, and all the unperturbed quantities are again evaluated at $x = x_0$. In the present work, we assume that $O(\eta_i) = 1$ so that L_n ($\simeq L_T$) is the typical macroscopic length of the system. It is known[19,20] that, in the case of the flat density profile ($L_n \gg L_T$), the η_i mode has different

properties. The appropriate nondimensional space-time variables are

$$\tilde{x}=\frac{x-x_0}{\rho_s},\quad \tilde{y}=\frac{y}{\rho_s},\quad \tilde{z}=\frac{z}{L_n},\quad \tau=\frac{tc_s}{L_n}.$$

Assuming that the fluctuation level is small in the sense that the ratios $\tilde{n}/n_0, \tilde{v}_\parallel/c_s, \tilde{p}_i/p_{i0}$, and $e\tilde{\Phi}/T_e$ are of order of ρ_s/L_n, and the fluctuating quantities vary more rapidly in space than the corresponding unperturbed quantities, the nonlinear evolution equations of the fluctuations are given by

$$(1-\nabla_\perp^2)\frac{\partial\phi}{\partial\tau}=-(1+K\nabla_\perp^2)\frac{\partial\phi}{\partial\tilde{y}}-\nabla_\parallel v+\{\phi,\nabla_\perp^2\phi\}-\mu_\perp\nabla_\perp^4\phi, \tag{5}$$

$$\frac{\partial v}{\partial\tau}=-\nabla_\parallel(\phi+p)-\{\phi,v\}+\mu_\perp\nabla_\perp^2 v+\mu_\parallel\nabla_\parallel^2 v, \tag{6}$$

$$\frac{\partial p}{\partial\tau}=-K\frac{\partial\phi}{\partial\tilde{y}}-\Gamma\nabla_\parallel v-\{\phi,p\}+\chi_\perp\nabla_\perp^2 p+\chi_\parallel\nabla_\parallel^2 p, \tag{7}$$

where only the $\mathbf{E}\times\mathbf{B}$ convective nonlinear terms are retained as nonlinearity for simplicity. It is shown in Ref. 7 that the other nonlinearities arising from $v_\parallel\nabla_\parallel\mathbf{v}$ and $v_\parallel\nabla_\parallel p$ are negligible if $\rho_s \ll L_n, L_T$. Here the dependent variables are defined by

$$\phi=(e\tilde{\Phi}/T_e)(L_n/\rho_s),$$
$$v=(\tilde{v}_\parallel/c_s)(L_n/\rho_s),$$
$$p=(\tilde{p}_i/p_{i0})(L_n/\rho_s)(T_i/T_e),$$

all of which are of order of unity, the Poisson bracket $\{f,g\}$ and the perpendicular gradient $\nabla_\perp$ are defined by

$$\{f,g\}=\hat{\mathbf{z}}\cdot\nabla_\perp f\times\nabla_\perp g=\frac{\partial f}{\partial\tilde{x}}\frac{\partial g}{\partial\tilde{y}}-\frac{\partial f}{\partial\tilde{y}}\frac{\partial g}{\partial\tilde{x}},$$

$$\nabla_\perp=\frac{\partial}{\partial\tilde{x}}\hat{\mathbf{x}}+\frac{\partial}{\partial\tilde{y}}\hat{\mathbf{y}}. \tag{8}$$

In deriving Eqs. (5)–(7), the magnetic field is assumed to take the form

$$\mathbf{B}=B\{\hat{\mathbf{z}}+[(x-x_0)/L_s]\hat{\mathbf{y}}\},$$

where L_s is the shear length. With the definition of the shear parameter $s=L_n/L_s$, the parallel derivative $\nabla_\parallel$ in Eqs. (5)–(7) may be written as

$$\nabla_\parallel=\frac{\partial}{\partial\tilde{z}}+s\tilde{x}\frac{\partial}{\partial\tilde{y}}. \tag{9}$$

The constants $\mu_{\perp,\parallel}$ and $\chi_{\perp,\parallel}$ in Eqs. (5)–(7) are appropriately chosen dissipation rates. For a collisional plasma the values of μ and χ may be taken from the Coulomb transport theory.[18] For the high-temperature tokamak plasmas of interest the appropriate choice of $\mu_\parallel$ and $\chi_\parallel$ is to model the collisionless ion Landau effect.

The domain on which Eqs. (5)–(7) are solved is given by the cubic box $|\tilde{x}|\leqslant L_x$, $0\leqslant\tilde{y}\leqslant L_y$ and $0\leqslant\tilde{z}\leqslant L_z$, L_y and L_z being constants of order unity. The size of the box in the x direction L_x is taken to be large enough, so that when there is magnetic shear ($s\neq 0$), single helicity modes localized at $\tilde{x}=0$ decay sufficiently as $|\tilde{x}|\to L_x$. In the case of zero shear $2L_x$ represents the width of the constant background ion pressure gradient and/or the constant background density gradient. For the boundary conditions of Eqs. (5)–(7), all the dependent variables are assumed to vanish at $|\tilde{x}|=L_x$ and to be periodic in the $\tilde{y}$ and $\tilde{z}$ directions.

We define the space average $\langle\ \rangle$ by

$$\langle\ \rangle=\frac{1}{2L_xL_yL_z}\int_{-L_x}^{L_x}d\tilde{x}\int_0^{L_y}d\tilde{y}\int_0^{L_z}d\tilde{z}, \tag{10}$$

and we introduce the averaged fluctuation energy densities

$$E_\phi=\tfrac{1}{2}\langle\phi^2+|\nabla_\perp\phi|^2\rangle,$$
$$E_v=\tfrac{1}{2}\langle v^2\rangle,\quad\text{and}\quad E_p=\tfrac{1}{2}\langle p^2\rangle.$$

The energy transfer rates between the three energy densities are given by the compressional work $W_{\rm comp}$ done by $\nabla_\parallel v$,

$$W_{\rm comp}=\langle p\nabla_\parallel v\rangle,$$

and the $j_\parallel E_\parallel$ work done on the parallel ion current $j_\parallel\equiv ev_\parallel$,

$$W_{jE}=-\langle v\nabla_\parallel\phi\rangle.$$

It follows from Eqs. (5)–(7) that the energy transfer equations are given by

$$\frac{dE_\phi}{dt}=-W_{jE}-\mu_\perp\langle|\nabla_\perp^2\phi|^2\rangle,$$

$$\frac{dE_v}{dt}=W_{jE}+W_{\rm comp}-\mu_\perp\langle|\nabla_\perp v|^2\rangle-\mu_\parallel\langle(\nabla_\parallel v)^2\rangle,$$

and

$$\frac{dE_p}{dt}=KQ-\Gamma W_{\rm comp}-\chi_\perp\langle|\nabla_\perp p|^2\rangle-\chi_\parallel\langle(\nabla_\parallel p)^2\rangle,$$

where

$$Q=\left\langle p\frac{\partial\phi}{\partial y}\right\rangle=-\left(\frac{\rho_s}{L_n}\frac{cT_e}{eB}\frac{p_{i0}}{L_n}\frac{T_e}{T_i}\right)^{-1}\langle\tilde{p}_i\tilde{v}_{Ex}\rangle \tag{11}$$

is the anomalous ion heat flux across the magnetic flux surface and $\tilde{v}_{Ex}=\mathbf{v}_E\cdot\nabla x$. These anomalous transfers W_{jE} and $W_{\rm comp}$ take energy out of the thermal ions and produce a growth of E_p, E_v, and E_ϕ. The source of the turbulence arises from the unperturbed ion pressure gradient

$$K=-\frac{dp_{i0}}{dx}\frac{L_n}{n_0T_e}=\frac{T_i}{T_e}(1+\eta_i),$$

which drives the total fluctuation energy density

$$E_T=E_\phi+E_v+(1/\Gamma)E_p \tag{12}$$

with

$$\frac{dE_T}{dt}=\frac{KQ}{\Gamma}-\sum_\alpha P_\alpha, \tag{13}$$

where P_α are the dissipation rates given by

$$P_1=\mu_\perp\langle|\nabla_\perp^2\phi|^2\rangle,\quad P_2=\mu_\perp\langle|\nabla_\perp v|^2\rangle,$$
$$P_3=\mu_\parallel\langle|\nabla_\parallel v|^2\rangle,\quad P_4=(\chi_\perp/\Gamma)\langle|\nabla_\perp p|^2\rangle,$$
$$P_5=(\chi_\parallel/\Gamma)\langle|\nabla_\parallel p|^2\rangle.$$

In the turbulent steady state the free-energy production KQ/Γ is balanced by the energy absorption given by $\Sigma_\alpha P_\alpha$ in Eq. (13).

III. LINEAR STABILITY THEORY AND MIXING LENGTH THEORY

Having presented the dynamical equations of the η_i mode in the preceding section, we examine linear properties of the system, especially focusing on the shear stabilization effect associated with plasma compressibility and parallel diffusion. We also attempt to clarify the physical meaning of the η_i mode using the local approximation of the linearized system, which will serve as the basis of physical interpretation of our conclusions discussed in Sec. VI.

A. Local stability theory

In the local approximation, in which $\partial/\partial\tilde{x}$ and $\nabla_\parallel$ are replaced by constants $i\tilde{k}_x$ and $i\tilde{k}_\parallel$, respectively, the linear dynamics of Eqs. (5)–(7) is given by the dispersion relation

$$(1+\tilde{k}_\perp^2)\tilde{\omega}^2-\tilde{k}_y\tilde{\omega}(1-K\tilde{k}_\perp^2)-\frac{\tilde{k}_\parallel^2(1+K\tilde{k}_y/\tilde{\omega})}{1-\Gamma\tilde{k}_\parallel^2/\tilde{\omega}^2}=0. \tag{14}$$

Here $\tilde{y}$, $\tilde{z}$, and τ dependence of the independent variables are assumed to be $\exp i(\tilde{k}_y\tilde{y}+\tilde{k}_z\tilde{z}-\tilde{\omega}\tau)$ and $\tilde{k}_\perp^2=\tilde{k}_x^2+\tilde{k}_y^2$. All the diffusion coefficients in Eqs. (5)–(7) are ignored in Eq. (14) for simplicity in the weakly dissipative, long-wavelength region. In the local approximation, the constant $\tilde{k}_\parallel$ models $\nabla_\parallel$ with the relation $\tilde{k}_\parallel=s\Delta_x\tilde{k}_y+\tilde{k}_z$, where Δ_x denotes a typical mode width in the x direction. When the shear s is small, the parallel derivative $\nabla_\parallel$ is approximately given by the constant $\tilde{k}_z$ and the dispersion relation of the linearized system of Eqs. (5)–(7) is also approximately given by Eq. (14). In this case, the parallel dynamics is dominated by the effect of the periodicity in the $\tilde{z}$ direction rather than the $\tilde{y}$ direction. In the case of zero shear, Eq. (14) becomes the exact dispersion relation of the linearized system of Eqs. (5)–(7) with the relation $\tilde{k}_\parallel=\tilde{k}_z$.

In the dimensional form, Eq. (14) may be written as

$$(1+k_\perp^2\rho_s^2)\omega^2-\omega\omega_e^*(1-Kk_\perp^2\rho_s^2)-\frac{k_\parallel^2c_s^2(1-\omega_{pi}^*/\omega)}{1-\Gamma k_\parallel^2c_s^2/\omega^2}=0, \tag{15}$$

where

$$\omega_e^*=(cT_e/eB)(k_y/L_n),$$
$$\omega_{pi}^*=-(cT_i/eB)(k_y/L_n)(1+\eta_i)=-\omega_e^*K,$$
$$k_\perp=\tilde{k}_\perp/\rho_s,\quad k_\parallel=\tilde{k}_\parallel/L_n,\quad \omega=c_s\tilde{\omega}/L_n.$$

Balancing the first term and the second term in Eq. (15) gives the dispersion of the drift wave, the frequency of which is downshifted from ω_e^* to

$$\omega_k^{\rm loc}=\omega_e^*(1-Kk_\perp^2\rho_s^2)/(1+k_\perp^2\rho_s^2), \tag{16}$$

for $|\omega_k^{\rm loc}|\gg\Gamma^{1/2}k_\parallel c_s$. The downshift of the local frequency in Eq. (16) is due to the perpendicular compressibility in the continuity equation. When the ion pressure gradient effect $Kk_\perp^2\rho_s^2$ is small, the wave traveling perpendicular to the field line propagates in the electron diamagnetic direction. The third term of Eq. (15) represents the ion acoustic wave coupled with the thermal mode arising from ω_{pi}^*. The modified sound velocity c_{sm} is given by

$$c_{sm}=c_s(1-\omega_{pi}^*/\omega)^{1/2},$$

where the finite Γ effect or the parallel compressibility in Eq. (15) is ignored. Since the local mode (16) has low frequency ($|\omega|\ll|\omega_{pi}^*|$) for $|\omega_{pi}^*|\sim\omega_e^*$, the modified sound velocity becomes complex as ω becomes complex, which is the manifestation of the η_i mode. We now estimate the growth rate from Eq. (15). For the mode with small perpendicular wave number $|k_\perp\rho_s|\ll K^{-1/2}$ and low frequency $|\omega|\ll\omega_e^*\sim|\omega_{pi}^*|$, the second and third terms in Eq. (15) become dominant, and the complex eigenfrequency is given by

$$\omega\simeq ik_\parallel c_s\sqrt{K}. \tag{17}$$

However, by choosing the wave number $k_\perp$ in such a way that the first term becomes more dominant than the second term in Eq. (15), i.e., $k_\perp\rho_s=K^{-1/2}$, we obtain the complex frequencies

$$\omega\simeq(-\omega_{pi}^*k_\parallel^2c_s^2)^{1/3},\quad[(-1\pm i\sqrt{3})/2](-\omega_{pi}^*k_\parallel^2c_s^2)^{1/3}, \tag{18}$$

by balancing the first term with the third term in Eq. (15). Since modes with small parallel wave numbers ($k_\parallel c_s\ll\omega_e^*$) are of interest, Eq. (18) gives a larger growth rate than Eq. (17).

The parallel and perpendicular diffusion coefficients in Eqs. (5)–(7) significantly stabilize the modes with high wave numbers. Taking into account the finite diffusion coefficients, we now solve numerically the more complicated dispersion relation obtained from Eqs. (5)–(7) under the local approximation. Figure 1 shows the contours of constant growth rate $\gamma=\mathrm{Im}\,\omega$ as a function of k_y and $k_\parallel$ with finite diffusion coefficients. Since the maximum growth rate generally occurs for finite k_x, k_x is chosen in such a way that $\gamma=\gamma(k_y,k_\parallel)$ takes its maximum value or $\gamma=\max_{k_x}\gamma(k_x,k_y,k_\parallel)$. In Fig. 1(a), where only the parallel diffusion coefficients $\mu_\parallel$ and $\chi_\parallel$ are taken to be finite, growth rate distribution on the $(k_y,k_\parallel)$ plane is more widespread in the k_y-direction than the growth rate in Fig. 1(b). In Fig. 1(b) the perpendicular diffusion coefficients $\mu_\perp$ and $\chi_\perp$ are also taken into account.

B. Eigenmode stability theory

Now we consider the eigenvalue problem in more detail without using the local approximation. The solutions of the linearized equations of the system (5)–(7) with the following forms are considered:

$$\phi=\tilde{\phi}(\tilde{x})\exp i(k\tilde{y}-\tilde{\omega}\tau),$$
$$v=\tilde{v}(\tilde{x})\exp i(k\tilde{y}-\tilde{\omega}\tau),$$
$$p=\tilde{p}(\tilde{x})\exp i(k\tilde{y}-\tilde{\omega}\tau),$$

where $\tilde{\omega}$, $\tilde{\phi}(x)$, $\tilde{v}(x)$, and $\tilde{p}(x)$ are assumed to take complex values and k denotes the real wave number $k=\tilde{k}_y$. The $\tilde{z}$ dependence of the solutions is ignored since, in the case of a finite shear s, the $\tilde{z}$ dependence of the linear solutions only shifts the position of their mode rational surfaces in the x direction. Assuming that $\mu_\perp=\chi_\perp=0$ in the system (5)–(7) for simplicity, the linearized equations of this system are reduced to the following eigenvalue problem:

$$\frac{d^2}{d\tilde{x}^2}\tilde{\phi}+\left(-k^2+\frac{1-\Omega}{\Omega+K}+\frac{B+K}{\Omega+K}\frac{s^2\tilde{x}^2}{AB-s^2\tilde{x}^2\Gamma}\right)\tilde{\phi}=0, \tag{19}$$

where

$$A=\Omega+i\mu_{\parallel}ks^2\tilde{x}^2,$$
$$B=\Omega+i\chi_{\parallel}ks^2\tilde{x}^2,$$

and $\Omega=\tilde{\omega}/k=\omega/\omega_e^*$. The relations of $\tilde{v}$ and $\tilde{p}$ to $\tilde{\phi}$ are given by

$$\tilde{v}=[s\tilde{x}(K+B)/(AB-s^2\tilde{x}^2\Gamma)]\tilde{\phi}$$

and

$$\tilde{p}=[(AK+s^2\tilde{x}^2\Gamma)/(AB-s^2\tilde{x}^2\Gamma)]\tilde{\phi}.$$

In this subsection, we only consider an ideal sheared slab or $L_x=\infty$. As discussed in Sec. II, therefore, the boundary condition of Eq. (19) is such that $|\tilde{\phi}(x)|\to 0$ as $|\tilde{x}|\to\infty$.

It is known[7] that, in the case where $\mu_{\parallel}=\chi_{\parallel}=\Gamma=0$, Eq. (19) gives the following eigenvalue Ω and the eigenfunction ϕ:

$$\Omega=[1/2(1+k^2)]\{[1-k^2K-is(2l+1)]\pm\sqrt{[1-k^2K-is(2l+1)]^2-4is(1+k^2)(2l+1)K}\} \tag{20}$$

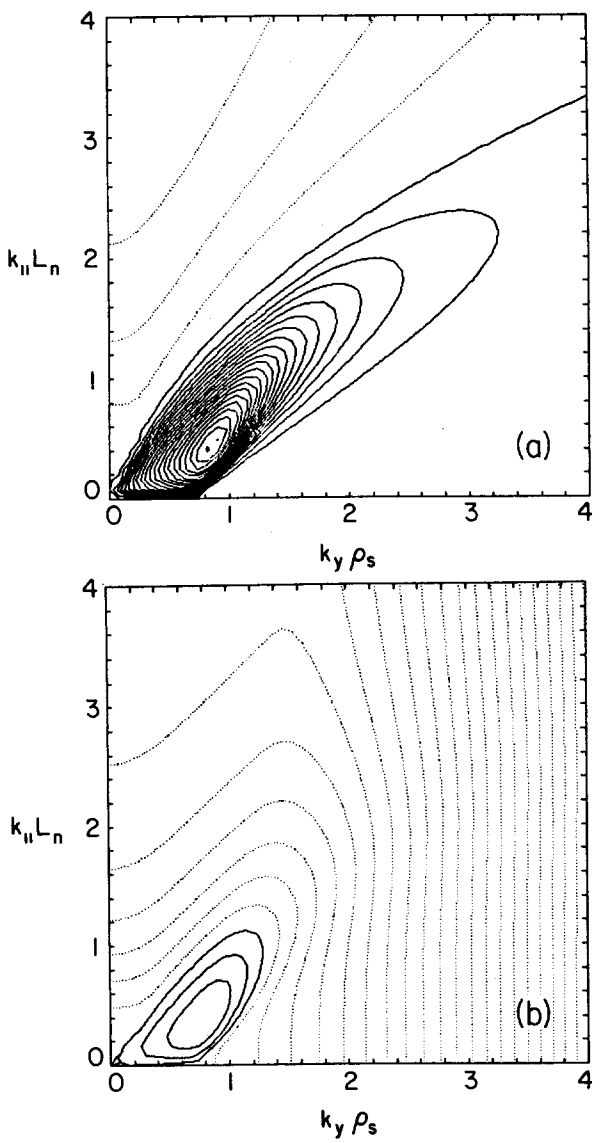

FIG. 1. The contours of constant linear growth rate γ as functions of k_y and $k_{\parallel}$ obtained from Eqs. (5)–(7) under the local assumption. Here k_x is chosen so as to maximize $\gamma=\gamma(k_x,k_y,k_{\parallel})$. The solid lines represent $\gamma\geqslant 0$ and the dotted lines represent $\gamma<0$. In (a), $K=3.0$, $\Gamma=2.0$, $\mu_{\parallel}=\chi_{\parallel}=1.0$, and $\mu_{\perp}=\chi_{\perp}=0$. The maximum of $\gamma=0.28c_s/L_n$ is obtained at $k_y\rho_s=0.82$ and $k_{\parallel}L_n=0.41$. The difference between the two contour lines indicates $\Delta\gamma=1.2\times10^{-2}c_s/L_n$. In (b), all the parameters are the same as those in (a) except $\mu_{\perp}=\chi_{\perp}=0.1$. The maximum of $\gamma=0.22\,c_s/L_n$ is obtained at $k_{\parallel}L_n=0.34$ and $k_y\rho_s=0.73$. The difference between the two contour lines indicates $\Delta\gamma=0.90\times10^{-2}c_s/L_n$.

and

$$\tilde{\phi}=e^{-\sigma\tilde{x}^2/2}H_l(\sigma^{1/2}\tilde{x}), \tag{21}$$

where $\sigma=is/\Omega$, $l(l\geqslant 0)$ is the radial mode number associated with the lth eigenvalue of the Weber equation, and $H_l(z)$ is the lth-order Hermitian function of the complex variable z.

Since the shear parameter s is generally a small number, we are able to reduce the expression for Ω in Eq. (20) to a simpler form in the following two limiting cases. First we consider the case where

$$|\tilde{s}/(1-k^2K)|\ll 1, \tag{22}$$

with $\tilde{s}=(2l+1)s$. Although we do not take any specific ordering of k^2, the condition above is in practice satisfied when $|k^2K|\ll 1$, so we assume $1-k^2K>0$ under this condition. We note that the mode under consideration is not the fastest growing mode. We also note that, in the local approximation, the condition (22) causes the balance between the second term and the third term of Eq. (14) or, in other words, strong coupling of the drift wave with the ion acoustic wave. In this case, the term given as the square root in the right-hand side of Eq. (20) is analytic at $s=0$. Therefore we expand Ω in terms of $\epsilon_1=\tilde{s}/(1-k^2K)$ around $\epsilon_1=0$. Taking up to the third order of ϵ_1, we obtain

$$\mathrm{Re}\,\Omega=-K\left(1+\frac{1+k^2}{1-k^2K}K\right)\left(\frac{(2l+1)s}{1-k^2K}\right)^2+O(\epsilon_1^4) \tag{23}$$

and

$$\mathrm{Im}\,\Omega=\frac{(2l+1)sK}{1-k^2K}-K\left(1+2\frac{1+k^2}{1-k^2K}K\right)\times\left(1+\frac{1+k^2}{1-k^2K}\right)\left(\frac{(2l+1)s}{1-k^2K}\right)^3+O(\epsilon_1^5). \tag{24}$$

A stabilizing effect of a larger shear s appears as the $O(\epsilon_1^3)$ correction in Eq. (24). It follows from Eqs. (23) and (24) that to the lowest order in ϵ_1, the fundamental mode ($l=0$) with a small wave number k is a purely growing mode with the complex eigenfrequency

$$\Omega=isK, \tag{25}$$

or $\omega=-i\omega_{pi}^*s$ ($\omega_{pi}^*<0$).

The maximum growth rate is, however, attained when $|1-k^2K|\ll 1$, as also seen in the local analysis. Unlike the

condition (22), under the condition

$$|1 - k^2K| \lesssim |\tilde{s}| \ll 1, \tag{26}$$

the square-root term of the right-hand side of Eq. (20) is no longer analytic at $s = 0$. We therefore expand the square-root term in terms of $(1 - k^2K + i\tilde{s})^2/i\tilde{s}(K + 1)$ and obtain both maximum Im Ω and maximum growth rate $\tilde{\gamma}$:

$$\text{Im}\,\Omega = \frac{K}{2}\left(\sqrt{\frac{2(2l+1)s}{K+1}} - \frac{(2l+1)s}{K+1} + O(\epsilon_2^{3/2})\right), \tag{27}$$

$$\tilde{\gamma} = k\,\text{Im}\,\Omega = \frac{\sqrt{K}}{2}\left(\sqrt{\frac{2(2l+1)s}{K+1}} - \frac{(2l+1)s}{K+1} + O(\epsilon_2^{3/2})\right), \tag{28}$$

at

$$k^2 = 1/K + O(\epsilon_2). \tag{29}$$

The real frequency at this wave number k is given by

$$\text{Re}\,\Omega = \frac{K}{2}\left(-\sqrt{\frac{2(2l+1)s}{K+1}} - \frac{3(2l+1)s}{K+1} + O(\epsilon_2^{3/2})\right). \tag{30}$$

Here $\epsilon_2 = (2l + 1)s/(K + 1)$. For the fundamental mode ($l = 0$) with large K, we obtain the familiar formulas[7]

$$\text{Im}\,\Omega \simeq \sqrt{sK/2}$$

and

$$\text{Re}\,\Omega \simeq -\sqrt{sK/2}, \tag{31}$$

to the lowest order of s. In the dimensional form, the complex eigenfrequency is given by $\omega = (-1 + i)\sqrt{s/2} \times (c_s/L_n)$, i.e., independent of K to the lowest order of s. Under the condition (26) the instability obtained here is more due to the balance between the first term and the third term of Eq. (14) or the destabilization of the ion acoustic wave by the thermal mode, rather than the coupling of the drift wave with the destabilized ion acoustic wave.

So far we have considered the case where the radial number l is small enough so that either Eq. (22) or Eq. (26) holds. However, as shown in Eqs. (24) and (27), larger radial eigenmode number l tends to increase the growth rate when the shear s is small. Since the dependence of Ω in Eq. (20) on l is given by its dependence on $\tilde{s} = (2l + 1)s$, we plot the growth rate $\gamma = \text{Im}\,\tilde{\omega} = k\,\text{Im}\,\Omega$ as a function of $\tilde{s}$ and k in Fig. 2. Here $k = 0.2m$ and $K = 3.0$. The maximum of $\gamma_{\max} = 0.753$ is obtained at $\tilde{s} = \tilde{s}_{\max} = 0.75$ and $k = 1.4$ (or $m = 7$). As a function of small shear $s (s \ll 1)$, the growth rate γ remains constant at its maximum $\gamma_{\max}$ since, as s (not $\tilde{s}$) decreases, the radial eigenmode number l increases so as to keep $\tilde{s} = (2l + 1)s$ at the constant value $s = \tilde{s}_{\max}$. Figure 3 shows the dependence of γ on s (not $\tilde{s}$) calculated from Eq. (20) when $K = 3.0$. Here l and m (or k) are chosen to maximize the growth rate γ. It is shown that the $l = 0$ mode is dominant when $s \gtrsim 4.1$ and the $l = 1$ mode is dominant when $1.8 \lesssim s \lesssim 4.1$. For $s = 0.1$, which is a typical shear parameter of

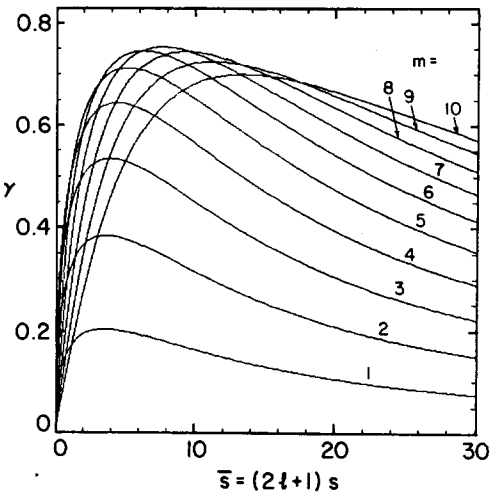

FIG. 2. The growth rate γ (normalized by c_s/L_n) as a function of $\tilde{s} = (2l + 1)s$ and $k = k_y\rho_s$ calculated from Eq. (20). The parameters are $K = 3.0$, $k = 0.2m$ ($1 \lesssim m \lesssim 10$), and $\Gamma = \mu_\parallel = \chi_\parallel = \mu_\perp = \chi_\perp = 0$. The growth rate γ attains its maximum value 0.753 c_s/L_n at $\tilde{s} = 7.65$ and $k = 1.4$.

a tokamak plasma, the radial eigenmode number is given by $l = 38$ when $K = 3$. We note that this unrealistically high radial eigenmode number l is reduced when the effect of finite Γ and finite diffusion are taken into account, as will be shown later.

Returning to the original eigenvalue problem of Eq. (19), we now seek the stabilizing effects of the compressibility of the parallel flow (i.e., $\Gamma \neq 0$) and the parallel diffusion (i.e., $\mu_\parallel, \chi_\parallel \neq 0$). It should be noted that by using nonzero values of $\mu_\parallel$ and $\chi_\parallel$, we are able to avoid the singularity of the last term of Eq. (19) arising from the finite value of Γ. Assuming that $s^2\Gamma, |\mu_\parallel ks^2|$ and $|\chi_\parallel ks^2|$ are small, we expand

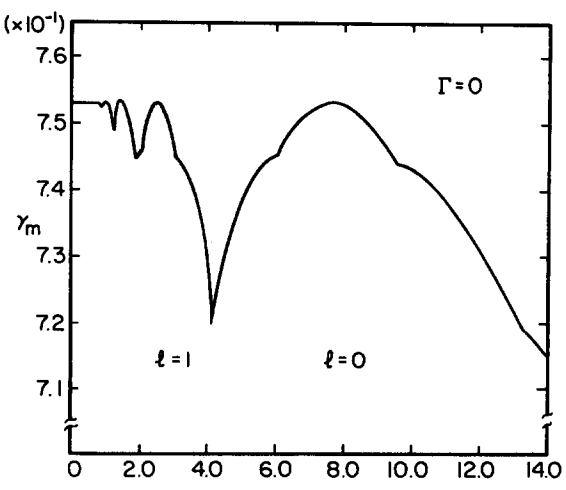

FIG. 3. The largest growth rate γ_m (normalized by c_s/L_n) as a function of the shear s, calculated from Eq. (20). All the parameters used here are the same as those in Fig. 2. The mode numbers l and m are chosen so as to maximize γ. For $s \gtrsim 4.1$, the $l = 0$ mode is dominant and for $1.8 \lesssim s \lesssim 4.1$, the $l = 1$ mode is dominant.

the last term of the left-hand side of Eq. (19) as a Taylor series in x. Here we also assume that the mode is localized near $x=0$, or more precisely, we solve Eq. (19) on a finite domain of $x(|x|\leqslant L_x)$ with the boundary conditions that $|\tilde{\phi}|=0$ at $|x|=L_x$. Therefore, by taking the values of $s^2\Gamma$, $|\mu_\parallel k s^2|$, and $|\chi_\parallel k s^2|$ to be small enough, the Taylor expansion is uniformly convergent. The size of the domain L_x, however, is taken to be large enough, so that the lowest-order solution of Eq. (19) is well approximated by Eq. (21) with the eigenvalue Eq. (20).

Writing Ω as the sum of the lowest-order growth rate Ω_0 given by the right-hand side of Eq. (20) and the remainder Ω_1, where $|\Omega_1/\Omega_0|$ is also assumed to be small, we expand Eq. (19) in terms of these small parameters. Retaining up to the term of $\tilde{x}^4$, we obtain

$$\frac{d^2\tilde{\phi}}{d\tilde{x}^2}+[E_0+E_1-V_0(\tilde{x})-V_1(\tilde{x})]\tilde{\phi}=0, \tag{32}$$

where

$$\begin{aligned} E_0&=-k^2+(1-\Omega_0)/(\Omega_0+K),\\ E_1&=-[(K+1)/(\Omega_0+K)^2]\Omega_1,\\ V_0&=-s^2\tilde{x}^2/\Omega_0^2,\\ V_1&=(1/\Omega_0^2)[(2\Omega_1/\Omega_0)s^2\tilde{x}^2-Ds^4\tilde{x}^4], \end{aligned} \tag{33}$$

and

$$D=\frac{\Gamma}{\Omega_0^2}-\frac{i(\mu_\parallel+\chi_\parallel)k}{\Omega_0}+\frac{i\chi_\parallel k}{\Omega_0+K}.$$

To the lowest order, Eq. (32) becomes Eq. (19) or

$$\frac{d^2\tilde{\phi}_0}{dx^2}+[E_0-V_0(x)]\tilde{\phi}_0=0, \tag{34}$$

where we expand $\tilde{\phi}$ as

$$\tilde{\phi}=\tilde{\phi}_0+\tilde{\phi}_1+\cdots. \tag{35}$$

The lth eigenvalue $\Omega_0=\Omega_0^{(l)}$ and the lth eigenfunction $\tilde{\phi}_0=\tilde{\phi}_0^{(l)}$ of Eq. (34) are given by Eqs. (20) and (21), respectively. From the next-order equation and using the solvability condition of the inhomogeneous equation, we obtain the following relation:

$$E_1=\int_{-\infty}^{\infty}V_1(\tilde{x})\phi_0^{(l)2}\,d\tilde{x}\left(\int_{-\infty}^{\infty}\phi_0^{(l)2}\,d\tilde{x}\right)^{-1}, \tag{36}$$

where the integral is taken over the total domain (i.e., $|\tilde{x}|\leqslant L_x$ in the case of the finite domain). Using Eq. (21) as $\phi_0^{(l)}$, we rewrite Eq. (36) as

$$E_1=-D(s^4/\Omega_0^2\sigma_2)A_l+(2s^2\Omega_1/\Omega_0^3\sigma)B_l, \tag{37}$$

where

$$A_l=\frac{1}{\sqrt{\pi}2^l l!}\int_{-\infty}^{\infty}\xi^4 e^{-\xi^2}H_l^2(\xi)d\xi=\frac{3}{4}(2l^2+2l+1)$$

and

$$B_l=\frac{1}{\sqrt{\pi}2^l l!}\int_{-\infty}^{\infty}\xi^2 e^{-\xi^2}H_l^2(\xi)d\xi=\frac{1}{2}(2l+1).$$

Equating Eqs. (33) and (37) and solving the resulting equation for Ω_1 yields

$$\Omega_1^{(l)}=-s^2DA_l\left(\frac{K+1}{(\Omega_0+K)^2}-2i\frac{sB_l}{\Omega_0^2}\right)^{-1}, \tag{38}$$

which is the first-order correction to the lth eigenvalue $\Omega_0^{(l)}$.

In order to observe the stabilizing effects arising from finite values of $\mu_\parallel$, $\chi_\parallel$, and Γ, we further simplify Eq. (38) under the assumption (22) or $|\epsilon_1|\ll 1$. Since Eq. (38) gives a $|s|^2$ order correction to the unperturbed eigenvalue $\Omega_0^{(l)}$, we need the expression of Im $\Omega_0^{(l)}$ correct up to $O(\epsilon_1^2)$:

$$\text{Im }\Omega_0^{(l)}=\frac{(2l+1)sK}{1-k^2K}+O(\epsilon_1^3).$$

Substituting this expression to Eq. (38) and keeping the terms up to $O(\epsilon_1^2)$, Eq. (38) becomes

$$\text{Re }\Omega_1^{(l)}=\frac{3}{4}(2l^2+2l+1)\frac{(K+1)\Gamma s^2}{(1-k^2K)^2}+O(\epsilon_1^3)$$

and

$$\text{Im }\Omega_1^{(l)}=-\frac{3(2l^2+2l+1)}{4(2l+1)}s\times\left(\Gamma+k(\mu_\parallel+\chi_\parallel)\frac{(2l+1)Ks}{1-k^2K}\right)+O(\epsilon_1^3).$$

Therefore the growth rate of the mode Im $\Omega^{(l)}=$ Im $\Omega_0^{(l)}+$ Im $\Omega_1^{(l)}$ is given to $O(\epsilon_1^2)$ by

$$\text{Im }\Omega^{(l)}=(2l+1)s\left[\frac{K}{1-k^2K}-\frac{3}{4}\frac{(2l^2+2l+1)}{(2l+1)^2}\times\left(\Gamma+k(\mu_\parallel+\chi_\parallel)\frac{(2l+1)Ks}{1-k^2K}\right)\right]. \tag{39}$$

It follows that in the case of $l=0$ and small k^2, Eq. (39) is reduced to

$$\text{Im }\Omega^{(0)}=s[K-\tfrac{3}{4}\Gamma-\tfrac{3}{4}k(\mu_\parallel+\chi_\parallel)Ks] \tag{40}$$

to the lowest order of k^2. We thus find from Eq. (40) that the growth rate is reduced by the compressibility of the parallel flow (i.e., nonzero Γ) and parallel diffusions (i.e., nonzero $\mu_\parallel$ and $\chi_\parallel$). We, however, note that Eqs. (39) and (40) are valid only for a specific k that may vary in the small range $0\leqslant k^2\ll 1/K$. Therefore, the expressions of the growth rate given in these equations do not represent the general k dependence of the growth rate. We also note that the radial eigenmode number l and the wave number k are fixed in the above calculations. Figures 4(a) and 4(b) show Im Ω of Eq. (40) as a function of K and s, respectively, as well as the exact eigenvalues Im Ω obtained from Eq. (19) with the use of a shooting code.

Although Eqs. (39) and (40) are derived under the assumption that the stabilizing terms associated with Γ, $\mu_\parallel$ and $\chi_\parallel$ are small, we extrapolate the result to the case where the second and third terms in the parentheses of Eq. (40) are comparable to the first term K in order to estimate the critical value $K_c^{(0)}(k)$ of K for a given small wave number k. Setting Im $\Omega^{(0)}=0$ in Eq. (40), the critical value $K_c^{(0)}(k)$ is approximately given by

$$K_c^{(0)}(k)=\tfrac{3}{4}\Gamma[1+\tfrac{3}{4}k(\mu_\parallel+\chi_\parallel)s], \tag{41}$$

or, in terms of η_i, the equation above may be rewritten as

$$\eta_{i,c}^{(0)}(k_y\rho_s)=\frac{3}{4}\gamma-1+\frac{9}{16}\gamma\frac{(\nu_\parallel+m_i\kappa_\parallel)}{m_i n_0 c_s L_n}k_y\rho_s\left(\frac{L_n}{L_s}\right). \tag{42}$$

Here $\nu_\parallel$ and $\kappa_\parallel$ are the parallel viscosity and the parallel heat

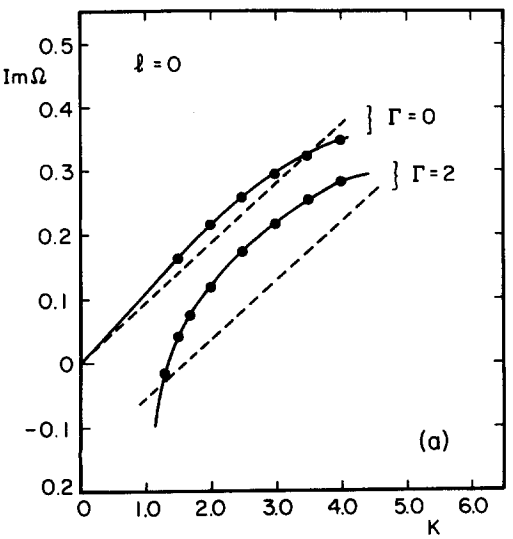

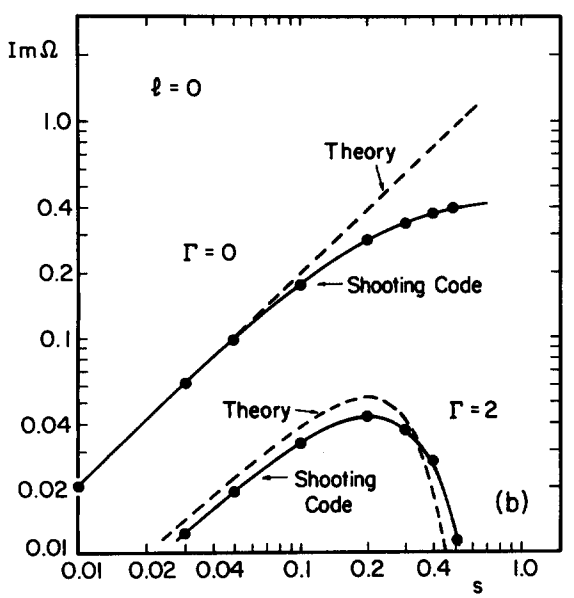

FIG. 4. The growth rates expressed by Im Ω for the fundamental ($l = 0$) mode with $\mu_\perp = \chi_\perp = 0$. The solid lines are obtained from the shooting code solving Eq. (19) and the broken lines from the theory [Eq. (39)]. The two cases, $\Gamma = 0$ and $\Gamma = 2$, are presented. (a) $\mu_\parallel = \chi_\parallel = 1.0$, $s = 0.1$, and $k = k_y\rho_s = 0.5$. (b) $\mu_\parallel = \chi_\parallel = 2.0$, $K = 2.0$, and $k = 0.2$.

conductivity in the dimensional form, respectively, defined by $\nu_\parallel = m_i n_0 c_s L_n \mu_\parallel$ and $\kappa_\parallel = n_0 c_s L_n \chi_\parallel$. For example, in the case where $\gamma = 2$, $\mu_\parallel = \chi_\parallel = 2$, $k = k_y\rho_s = 0.5$, and $s = L_n/L_s = 0.3$, we have $\eta_{i,c}^{(0)}(k = 0.5) \simeq 1.2$. The critical value η_i of the mode, denoted by $\eta_{i,c}$, is the minimum value of $\eta_{i,c}^{(l)}(k)$, i.e., $\eta_{i,c} = \min_{l,k} \eta_{i,c}^{(l)}(k)$. As we noted, however, Eqs. (39) and (40) are valid only for a limited range of k and not appropriate to estimate $\eta_{i,c}$. The critical value $\eta_{i,c}$ may be obtained with the use of the unperturbed eigenvalue Ω_0 evaluated near $k = K^{-1/2}$ given in Eqs. (27) and (30) with an appropriate choice of l. However, we do not proceed to this calculation here since our objective in the perturbation analysis presented here is to demonstrate the stabilizing effects arising from Γ, $\mu_\parallel$, and $\chi_\parallel$, which is shown in Eq. (39).

C. Mixing length estimates

We now estimate the nonlinear saturation level of the η_i-mode turbulence using the linear properties obtained in this section. By means of the mixing length theory, the anomalous diffusion coefficient D is estimated as

$$D = \tilde{\gamma}\Delta_x^2, \tag{43}$$

where Δ_x is the typical mode width in the $\tilde{x}$ direction. We here use the following definition of Δ_x:

$$\Delta_x^{-2} = \left| \mathrm{Re}\left(\frac{\langle (\partial\phi/\partial\tilde{x})^2 \rangle}{\langle \phi^2 \rangle} \right) \right|. \tag{44}$$

For the lowest-order solution $\phi = \phi_0$ of Eq. (34), we obtain

$$\Delta_x^{-2} = |\mathrm{Re}[\lambda - \tfrac{1}{2}\sigma(2l + 1)]|, \tag{45}$$

where

$$\lambda = -k^2 + (1 - \Omega)/(\Omega + K). \tag{46}$$

Choosing the fundamental mode ($l = 0$) with a small wave number ($|k^2 K| \ll 1$), we obtain from Eqs. (25), (45) and (46)

$$D = 2ksK^2, \tag{47}$$

to the lowest order of s. In this case, the mode width $\Delta_x = \sqrt{2K}$ estimated from Eq. (45) does not depend on the shear s.

If we use, however, the most strongly excited mode to evaluate Eq. (45), we obtain a different scaling of D. To the lowest order of s, the fastest growing mode is obtained when $k \simeq K^{-1/2}$ and $(2l + 1)s = \tilde{s}_{\max}$, the growth rate of which is given by Eqs. (27) or $\mathrm{Im}\,\Omega \simeq \sqrt{(2l + 1)sK/2}$ if K is large. Here, as before, $\tilde{s}_{\max}$ denotes the value of $\tilde{s} = (2l + 1)s$ that maximizes Im Ω given by Eq. (20). With the use of this growth rate, the anomalous mixing length diffusion coefficient D is evaluated by

$$D = 2\sqrt{K}, \tag{48}$$

which is independent of the shear s. In this case, the mode width Δ_x of the fastest growing mode is given by

$$\Delta_x^{-2} = \tfrac{1}{2}\sqrt{(2l + 1)s/2K} \tag{49}$$

to the lowest order of s. For the fixed radial mode number l, Δ_x scales as $s^{-1/4}$ while with the choice of l such that $(2l + 1)s = \tilde{s}_{\max}$, Δ_x is independent of shear.

In more realistic cases of finite Γ and finite diffusion, we use the linear initial value code to obtain the growth rate of the fastest growing mode. Figure 5 shows the growth rate $\gamma = k\,\mathrm{Im}\,\Omega$ calculated from the initial value code as a function of the shear s, where $K = 3.0$, $\Gamma = 2$, $\mu_\parallel = \chi_\parallel = 1.0$, and $\mu_\perp = \chi_\perp = 0.01$. The linear initial value code used here is the same code as the nonlinear initial value code described in Sec. V except for the nonlinear terms dropped in these calculations. In Fig. 5, it is shown that the growth rate γ is approximately a decreasing function of s in contrast to γ in Fig. 3 which is almost constant when $s \lesssim 1$. Figure 6 shows the anomalous diffusion coefficients D calculated from the mixing length estimate $D = \tilde{\gamma}\Delta_x^2$ as a function of s. Here $\tilde{\gamma} = \gamma L_n/c_s$ and $\Delta_x^{-2} = \langle (d\phi/dx)^2 \rangle / \langle \phi^2 \rangle$ are evaluated by the linear initial value code with the real-valued function ϕ and the same parameters used in Fig. 5. With the effects of

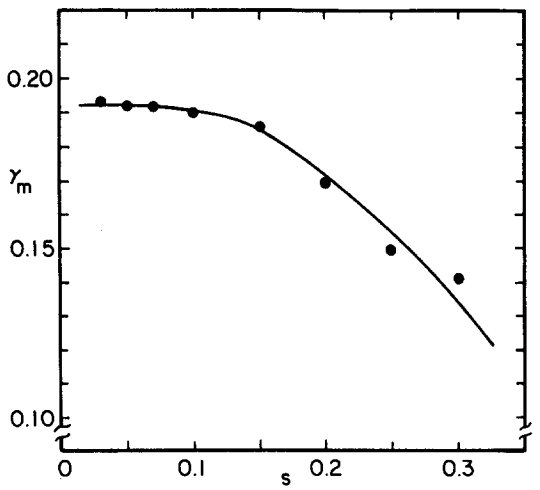

FIG. 5. The largest growth rate γ_m (normalized by c_s/L_n) as a function of s, calculated by the linear initial value code. The parameters used here are $K=3.0$, $\Gamma=2$, $\mu_\parallel=\chi_\parallel=1.0$, and $\mu_\perp=\chi_\perp=0.01$. The wave number $k=0.2m$ is chosen so as to maximize γ. Under these parameters, the $m=4$ mode is most strongly excited.

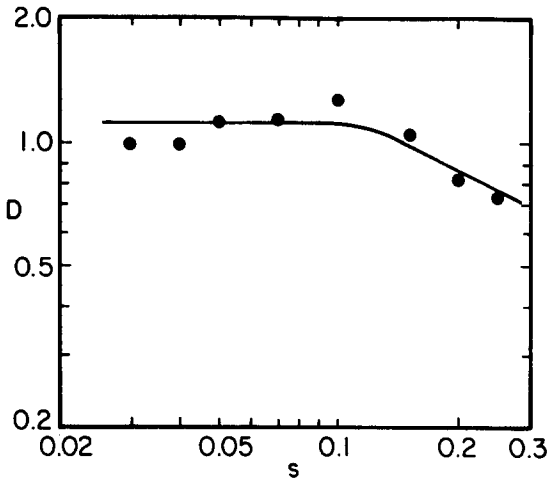

FIG. 6. The anomalous diffusion coefficients D as a function of s, calculated from the mixing length theory or $D=\tilde{\gamma}\Delta_x^2$. The linear growth rate $\tilde{\gamma}$ and the mode width Δ_x are evaluated from the most unstable linear mode obtained from the linear initial value code. The mode width Δ_x is defined by $\Delta_x^{-2}=\langle(d\phi/dx)^2\rangle/\langle\phi^2\rangle$. For $s\gtrsim 0.1$, D scales as $s^{-1/2}$.

finite Γ and finite diffusion, Fig. 6 shows weak dependence of D on s as $D\propto s^{-1/2}$ in contrast to Eq. (48). Taking into account this shear dependence of D forces the modification of Eq. (48) to become

$$D\propto (K/s)^{1/2}. \tag{50}$$

The previous work by Lee and Diamond[9] reports the scaling of the anomalous ion heat conductivity χ_i essentially identical to Eq. (47) while the previous work by Horton, Estes, and Biskamp[7] reports the scaling of χ_i similar to Eq. (50). As shown in this section and also as will be discussed in Sec. VI, the disagreement between these two previous results arises from the choice of the linear mode used to evaluate the nonlinear saturation levels; in Ref. 9, the fundamental mode with small $k_y\rho_s$ (i.e., $l=0$, $|k^2K|\ll 1$) is taken to be responsible for the nonlinear process while in Ref. 7 the most strongly excited mode is considered to be important. Since the mixing length theory does not provide information about such an *a priori* choice of linear modes important in the nonlinear process, we need to proceed to more rigorous analyses and numerical simulations.

IV. NONLINEAR THEORY: BIFURCATION NEAR THE THRESHOLD

We now derive the saturation amplitude of the nonlinear η_i mode and the associated anomalous heat flux as a function of the ion temperature gradient or η_i near its critical value $\eta_{i,c}$. The method used here is the amplitude expansion method,[21,22] in which we regard the nonlinearly saturated mode with small amplitude as bifurcation from a marginally stable state and expand the dynamical equations with respect to a small amplitude around the linear solutions.

For convenience, we rewrite the dynamical equations (5)–(7) as follows:

$$M\frac{\partial}{\partial\tau}\psi+\mathcal{L}(K)\psi+N(\psi,\psi)=0, \tag{51}$$

where

$$\psi=\begin{pmatrix}\phi\\ v\\ p\end{pmatrix},$$

$$\mathcal{L}(K)=L_1+KL_2,\quad M=\begin{pmatrix}1-\Delta_\perp & 0 & 0\\ 0 & 1 & 0\\ 0 & 0 & 1\end{pmatrix},$$

$$L_1=\begin{pmatrix}\partial/\partial\tilde{y}+\mu_\perp\nabla_\perp^4 & \nabla_\parallel & 0\\ \nabla_\parallel & -\mu_\parallel\nabla_\parallel^2-\mu_\perp\nabla_\perp^2 & \nabla_\parallel\\ 0 & \Gamma\nabla_\parallel & -\chi_\parallel\nabla_\parallel^2-\chi_\perp\nabla_\perp^2\end{pmatrix},\quad L_2=\begin{pmatrix}\nabla_\perp^2\partial/\partial\tilde{y} & 0 & 0\\ 0 & 0 & 0\\ \partial/\partial y & 0 & 0\end{pmatrix}.$$

The nonlinear vector term $N(\psi,\psi)$ is defined as

$$N(f,g)=\begin{pmatrix} -\{f_1,\nabla_1^2 g_1\} \\ \{f_1,g_2\} \\ \{f_1,g_3\} \end{pmatrix}$$

for $f=(f_1,f_2,f_3)^T$ and $g=(g_1,g_2,g_3)^T$, where the superscript T denotes the transpose of the matrix. The linear analysis in Sec. II shows that Eq. (51) generally has a time periodic solution in the zero amplitude limit. We therefore expect that there also exists a time periodic solution at the marginally stable state to the nonlinear system (51), the period of which is generally a function of the amplitude. For a sufficiently small amplitude ϵ we search for the nonlinear solution ψ of Eq. (51) by expansion in ϵ. We therefore introduce the new variables

$$\begin{aligned} &\psi=\epsilon u(\mathbf{x},s), \\ &s=\omega(\epsilon)\tau, \end{aligned} \tag{52}$$

such that u is 2π periodic in s or $u(\mathbf{x},s+2\pi)=u(\mathbf{x},s)$. Here ϵ is the amplitude of the mode defined by

$$\epsilon^2=\frac{1}{2\pi V}\int_0^{2\pi} ds\int_V d\mathbf{x}|\psi|^2, \tag{53}$$

where $\mathbf{x}=(\tilde{x},\tilde{y},\tilde{z})$, V is the total volume of the domain defined in Sec. II, and $|\psi|^2=|\phi|^2+|v|^2+|p|^2$. Considering a set of functions $H=\{f(\mathbf{x},s)=(f_1,f_2,f_3)^T\}$, where $f_i=f_i(\mathbf{x},s)(1\leqslant i\leqslant 3)$ is 2π periodic in s and satisfies the boundary conditions given in Sec. II [and has appropriate regularities in $(\mathbf{x},s)$], we define the inner product of $f,g\in H$ as

$$\langle f,g\rangle=\frac{1}{2\pi V}\int_0^{2\pi} ds\int_V dx\, f\cdot g^*.$$

Here g^* denotes the complex conjugate of g and $f\cdot g^*=\Sigma_i f_i g_i^*(1\leqslant i\leqslant 3)$. Clearly $u(\mathbf{x},s)$ defined in Eq. (52) is an element of H. Using Eqs. (51)–(53), we have

$$\begin{aligned} &\omega(\epsilon)M\frac{\partial u}{\partial s}+\mathscr{L}(K)u+\epsilon N(u,u)=0, \\ &\|u\|=1,\quad u\in H, \end{aligned} \tag{54}$$

where $\|u\|=\langle u,u\rangle^{1/2}$. The goal of the analysis in this section is to solve Eq. (54) in the limit of small ϵ.

In the case of $\epsilon=0$, Eq. (54) reduces to the linear system discussed in Sec. III, the solution of which exists only when K satisfies the dispersion relation, i.e., $K=K_0(\omega)$. We therefore expect that also for nonzero ϵ, Eq. (54) has a solution only when K and $\omega(\epsilon)$ satisfy a certain relation or K is a function of ϵ. Assuming that ω, K, and u are analytic functions of ϵ, we expand them as follows:

$$\begin{aligned} &\omega=\omega_0+\omega_1\epsilon+\omega_2\epsilon^2+\cdots, \\ &K=K_0+K_1\epsilon+K_2\epsilon^2+\cdots, \\ &u=u_0+u_1\epsilon+u_2\epsilon^2+\cdots, \end{aligned} \tag{55}$$

where

$$u_i=\begin{pmatrix}\phi_i\\ v_i\\ p_i\end{pmatrix}\quad (i\geqslant 0).$$

Substituting Eqs. (55) into Eq. (54), we obtain the linear equations to the lowest order

$$\mathscr{T}u_0=0, \tag{56}$$

$$\|u_0\|=1,\quad \text{and}\quad u_0\in H, \tag{57}$$

where $\mathscr{T}=\omega_0 M(\partial/\partial s)+\mathscr{L}_0$ and $\mathscr{L}_0=L_1+K_0L_2$. Since we are interested in a saturated state near the marginally stable state, we have

$$\operatorname{Im}\omega_i=0\quad (i\geqslant 0)$$

and

$$K_0=K_c.$$

It should be noted that, as discussed in Sec. III, the real frequency $\operatorname{Re}\omega_0$ does not vanish generally at the marginally stable state, and the growth rate $\operatorname{Im}\omega_0$ changes from negative to positive as K passes K_c from below, i.e.,

$$\left.\frac{d(\operatorname{Im}\omega_0)}{dK}\right|_{K=K_c}>0. \tag{58}$$

The two independent solutions of Eq. (56) are given by $u_0=e^{is}\xi$ and $e^{-is}\xi^*$, where ξ satisfies

$$\begin{aligned} &i\omega_0 M\xi+\mathscr{L}_0\xi=0, \\ &\|\xi\|=1. \end{aligned} \tag{59}$$

For simplicity we assume that there is a unique solution ξ of this system at the marginal stable state. Since a real-valued solution of Eq. (56) at the marginally stable state is of interest, we may choose $u_0=\operatorname{Re}(e^{is}\xi)=\frac{1}{2}(e^{is}\xi+e^{-is}\xi^*)$ without loss of generality.

To the next order of ϵ, we obtain from Eqs. (54) and (55)

$$\mathscr{T}u_1=b, \tag{60}$$

where

$$\begin{aligned} &b=-\omega_1 M\frac{\partial u_0}{\partial s}-K_1L_2u_0-N(u_0,u_0), \\ &\langle u_1,u_0\rangle=0,\quad \text{and}\quad u_1\in H. \end{aligned}$$

In order to write the solvability condition of Eq. (59), we need the solutions $u^\dagger$ of the equation

$$\mathscr{T}^\dagger u^\dagger=0, \tag{61}$$

where $\mathscr{T}^\dagger$ is the adjoint operator of $\mathscr{T}$. Since M is a Hermitian operator, $\mathscr{T}^\dagger$ is given by

$$\mathscr{T}^\dagger=-\omega_0 M\frac{\partial}{\partial s}+\mathscr{L}_0^\dagger,$$

where $\mathscr{L}_0^\dagger$ is the adjoint operator of $\mathscr{L}_0$. The two independent solutions of (60) are given by $e^{is}\xi^\dagger$ and $e^{-is}\xi^\dagger$, where $\xi^\dagger$ satisfies

$$-i\omega_0 M\xi^\dagger+\mathscr{L}_0^\dagger\xi^\dagger=0.$$

Writing the two solutions $u_{(1)}^\dagger=e^{is}\xi^\dagger$ and $u_{(2)}^\dagger=e^{-is}\xi^{*\dagger}$, the solvability condition of Eq. (60) is

$$\langle u_{(i)}^\dagger,b\rangle=0\quad (i=1,2). \tag{62}$$

From the s dependence of the term $N(v_0,v_0)$, it is easy to show that

$$\langle u_{(i)}^\dagger,N(u_0,u_0)\rangle=0\quad (i=1,2).$$

Therefore Eq. (61) becomes

$$\left\langle u_{(i)}^\dagger,\omega_1 M\frac{\partial}{\partial s}u_0+K_1L_2u_0\right\rangle=0\quad (i=1,2), \tag{63}$$

which determines ω_1 and K_1. Writing Eq. (63) in terms of ξ,

we obtain

$$i\omega_1\langle\xi^\dagger,M\xi\rangle + K_1\langle\xi^\dagger,L_2\xi\rangle = 0 \tag{64}$$

and its complex conjugate. Since the solution ξ of Eq. (59) exists only when ω_0 satisfies the dispersion relation with K, i.e., $\omega_0 = \omega_0(K)$ for the parameter K, differentiating Eq. (59) in terms of K yields

$$\left(i\frac{d\omega_0}{dK}M + L_2\right)\xi + (i\omega_0 M + \mathscr{L}_0)\frac{d\xi}{dK} = 0. \tag{65}$$

Evaluating Eq. (63) at $K = K_c$ and taking the inner product of $\xi^\dagger$ and Eq. (65), we obtain

$$i\left(\frac{d\omega_0}{dK}\right)_{K=K_c}\langle\xi^\dagger,M\xi\rangle + \langle\xi^\dagger,L_2\xi\rangle = 0, \tag{66}$$

where we used

$$\left\langle\xi^\dagger,(i\omega_0 M + \mathscr{L}_0)\frac{d\xi}{dK}\right\rangle$$

$$= \left\langle\frac{d\xi}{dK},(-i\omega_0 M + \mathscr{L}_0^\dagger)\xi^\dagger\right\rangle = 0.$$

From Eqs. (64) and (66), we obtain

$$\left[\omega_1 - K_1\left(\frac{d\omega_0}{dK}\right)_{K=K_c}\right]\langle\xi^\dagger,M\xi\rangle = 0. \tag{67}$$

Since Im ω_1 is taken to be 0 for the marginally stable state, it follows from Eqs. (58) and (67) that

$$\omega_1 = K_1 = 0.$$

To the order of ϵ^2, we derive from Eqs. (54) and (55)

$$\mathscr{T}u_2 = -\omega_2 M\frac{\partial}{\partial s}u_0 - K_2 L_2 u_0 - F_2, \tag{68}$$

where

$$F_2 = N(u_0,u_1) + N(u_1,u_0).$$

The solvability condition of Eq. (68) then becomes

$$\omega_2\left\langle u_{(i)}^\dagger,M\frac{\partial u_0}{\partial s}\right\rangle + K_2\langle u_{(i)}^\dagger,L_2 u_0\rangle + \langle u_1^\dagger,F_2\rangle = 0,$$

which may be further reduced to

$$i\left[\omega_2 - K_2\left(\frac{d\omega_0}{dK}\right)_{K=K_c}\right]\langle\xi^\dagger,M\xi\rangle + 2\langle u_{(1)}^\dagger,F_2\rangle = 0$$

and its complex conjugate, where we used Eq. (66). Separating this equation into the real and complex parts, we obtain

$$K_2 = -\mathrm{Re}\left(\frac{2\langle u_{(1)}^\dagger,F_2\rangle}{\langle\xi^\dagger,M\xi\rangle}\right)\left[\left(\frac{d(\mathrm{Im}\,\omega_0)}{dK}\right)_{K=K_c}\right]^{-1}$$

and

$$\omega_2 = K_2\left(\frac{d(\mathrm{Re}\,\omega_0)}{dK}\right)_{K=K_c} - \mathrm{Im}\left(\frac{2\langle u_{(1)}^\dagger,F_2\rangle}{\langle\xi^\dagger,M\xi\rangle}\right).$$

Using K_2 obtained above and the linear marginally stable solutions, we calculate the anomalous heat flux $\langle p\,\partial\phi/\partial y\rangle$ to its lowest order. Assuming that $K_2 \neq 0$, we have $K - K_c = K_2\epsilon^2$ to the lowest order. Therefore,

$$\left\langle p\frac{\partial\phi}{\partial\tilde{y}}\right\rangle = \epsilon^2\left\langle p_0\frac{\partial\phi_0}{\partial\tilde{y}}\right\rangle = \frac{1}{K_2}\left\langle p_0\frac{\partial\phi_0}{\partial\tilde{y}}\right\rangle(K - K_c), \tag{69}$$

where p_0 and ϕ_0 are the linear marginally stable solutions. We note that the coefficient $\langle p_0\,\partial\phi_0/\partial\tilde{y}\rangle/K_2$ of $(K - K_c)$ is a function of K_c and s but does not depend on K.

Thus we have derived the dependence of the anomalous heat flux $\langle p_0\,\partial\phi_0/\partial\tilde{y}\rangle$ on the ion pressure gradient K in the limit of small amplitude. The dependence of the anomalous heat flux on the shear parameter s is not clear from Eq. (69) since the linear solutions p_0 and ϕ_0 as well as K_2 are generally complicated functions of s. The shear dependence of the coefficient $\langle p_0\,\partial\phi_0/\partial\tilde{y}\rangle$ in Eq. (69) may be obtained by solving the linear equations (56) and (57) numerically. However, we now proceed to direct numerical simulations of Eqs. (5) and (6), rather than studying the shear dependence of Eq. (69) in detail. The numerical simulations of the original dynamical system presented in the next section give the dependence of the anomalous heat flux on the shear s as well as the ion pressure gradient K under much wider range of parameters than the method used in this section and check the validity of the analytical result given in Eq. (69).

V. NUMERICAL SIMULATIONS

In this section we report the results of numerical simulations of the η_i modes and compare the results with the analytical predictions presented in the previous sections. The initial value code used to solve the nonlinear partial differential equations (5)–(7) is developed from the HIB code.[23,24] In the initial value code, Fourier representation for the $\tilde{y}$ and $\tilde{z}$ variables and a finite difference scheme for the $\tilde{x}$ variable are employed. At each time step the dependent variables are advanced by means of the predictor–corrector method. The boundary condition is that all the physical variables are periodic in $\tilde{y}$ and $\tilde{z}$ with periods L_y and L_z, respectively, and they vanish at $|\tilde{x}| = L_x$, as discussed in Sec. II. We refer to the (m,n) mode of the Fourier representation as the mode whose $\tilde{y}$ and $\tilde{z}$ dependence is given by the phase $2\pi \times (m\tilde{y}/L_y - n\tilde{z}/L_z)$. The wave numbers $\tilde{k}_y$ and $\tilde{k}_z$ are thus given by $\tilde{k}_y = 2\pi m/L_y$ and $\tilde{k}_z = 2\pi n/L_z$. In the 2-D calculations of the nonlinear single helicity modes,the $\tilde{z}$ dependence of the mode is ignored and the relation $\nabla_\parallel = s\tilde{x}\,\partial/\partial\tilde{y}$ is used, which induces single helicity modes localized at $\tilde{x} = 0$. In the 3-D calculations, the rational surface of the (m,n) mode is at $\tilde{x} = nL_y/msL_z$ since

$$\nabla_\parallel \propto (msx/L_y - n/L_z) = (ms/L_y)(x - nL_y/msL_z)$$

for the (m,n) mode. As initial conditions, small perturbations are given to each (m,n) mode at $\tau = 0$.

The typical parameters used in the simulations are $\mu_\parallel = \chi_\parallel = 1.0$, $\mu_\perp = \chi_\perp = 0.01$ to 0.1, $\Gamma = 2$, $s = 0$ to 0.3, and $K = 0.4$ to 3.0. As noted in Sec. II, the parallel diffusion parameters $\mu_\parallel$ and $\chi_\parallel$ are chosen so as to model the collisionless ion Landau effect for high-temperature plasmas. The perpendicular diffusion coefficients $\mu_\perp$ and $\chi_\perp$, on the other hand, may be taken from the classical collisional transport theory.[11] Using the classical viscosity $\nu_\perp \sim nT_i/\omega_{ci}^2\tau_i$ and the classical heat conductivity $\kappa_\perp \sim T_i/m_i\omega_{ci}^2\tau_i$, the normalized perpendicular diffusion coefficients $\mu_\perp$ and $\chi_\perp$ of Eqs. (5)–(7) are given by

$$\mu_\perp = \frac{\nu_\perp L_n}{m_i n c_s \rho_s^2} \simeq \left(\frac{T_i}{T_e}\right)\frac{L_n}{c_s\tau_i}$$

and

$$\chi_\perp = \frac{\kappa_\perp L_n}{n c_s \rho_s^2} \simeq \left(\frac{T_i}{T_e}\right)\frac{L_n}{c_s \tau_i},$$

where τ_i denotes the ion collision time. For a hydrogen plasma with $L_n = 1\text{m}, T_i = T_e = 3.5$ keV, $n = 6.6\times 10^{19}\ \text{m}^{-3}$, and $Z_{\text{eff}} = 2$, we have $\mu_\perp \sim \chi_\perp \sim 0.012$. The shear parameter s may be related to the safety factor q of a toroidal plasma by $s = -\epsilon_a n_0 q'/n_0' q^2$, where ϵ_a is the inverse aspect ratio. Therefore, the parameters chosen for the following simulation results are in an appropriate range of the parameter space of current tokamak experiments.

We first present the results of 2-D simulations of nonlinear single helicity modes. The size of the domain used for the 2-D simulations is $L_x = 20\sim 40$ and $L_y = 10\pi$, so that the smallest finite wave number k_y of the $m = 1$ mode is given by $k_y \rho_s = 0.2$. The equally spaced 150 mesh points in the case of $L_x = 20$ and 300 mesh points in the case of $L_x = 40$ are used for discretization of the interval $-L_x \leqslant \tilde{x} \leqslant L_x$. We also employ the Fourier components of $0 \leqslant m \leqslant 6$–12, which is confirmed to give enough resolution of the saturated state. Figure 7 shows the time evolution of the total energy E_T [Eq. (12)] for $K = 3$ and $s = 0.1$, where the saturation of the modes is observed at $\tau \simeq 50$. The contours of constant potential at $\tau = 500$ under the same conditions are shown in Fig. 8. The constant potential contours are the streamlines of the $\mathbf{E}\times\mathbf{B}$ flow. For comparison the contours of constant potential at saturation with a larger shear $s = 0.5$ is also shown in Fig. 9. It is observed that the modes are more localized to the rational surface $\tilde{x} = 0$ in the case of strong shear while the modes are spread over a wide range of $\tilde{x}$ in Fig. 8 for weak shear. The saturation in the 2-D simulations presented in this section is mainly due to the flattening of the mean ion pressure gradient or the quasilinear saturation. Although the background ion pressure gradient K is kept as a constant parameter during each numerical simulation, the $m = n = 0$ mode of the perturbed pressure p evolves to cancel the background ion pressure gradient K, as shown in Fig. 10. Since the system (5)–(7) with the boundary conditions employed here does not have any external heat source nor allow cooling at $|\tilde{x}| = L_x$, the mean ion pressure gradient (i.e., the sum of the background ion pressure gradient and the gradient of the $m = n = 0$ mode of the perturbed pressure) cannot be maintained as a constant during the time evolution.

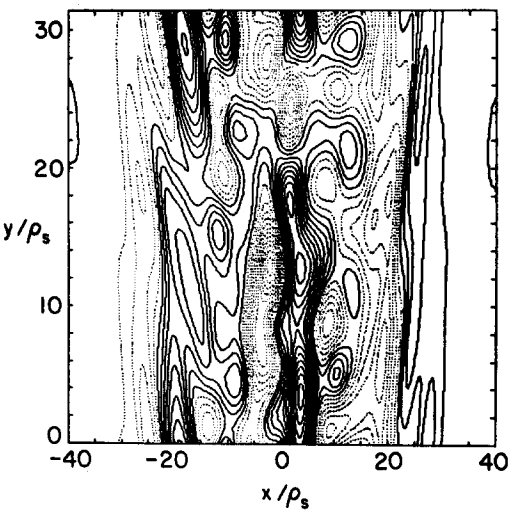

FIG. 8. The contours of constant ϕ at $\tau = tc_s/L_n = 500$, obtained from the long-time extension of the simulation shown in Fig. 7.

The anomalous ion heat conductivity χ_i is defined by

$$\chi_i = \frac{\overline{\langle \tilde{p}_i \tilde{v}_{ir} \rangle}}{-p_{i0}'} = -\frac{\rho_s}{L_n}\left(\frac{cT_e}{eB}\right)\overline{\left\langle p\frac{\partial \phi}{\partial y}\right\rangle} K^{-1}. \tag{70}$$

Here the time average $\overline{g(t)}$ of a time-dependent function $g(t)$ is defined by

$$\overline{g(t)} = \lim_{T\to\infty}\frac{1}{T}\int_0^T g(t)dt$$

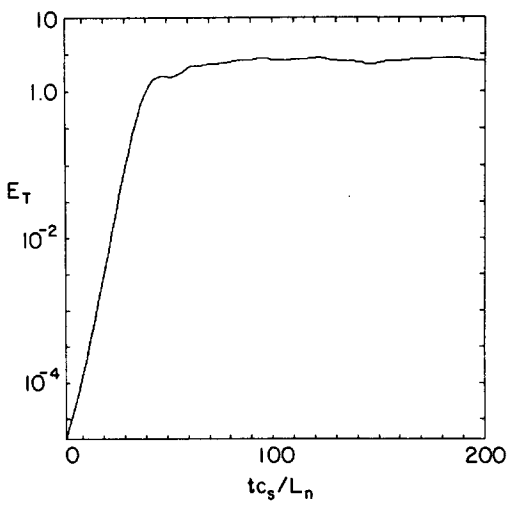

FIG. 7. Time evolution of the total energy E_T obtained from the single-helicity calculation, where $K = 3.0$, $s = 0.1$, $\Gamma = 2$, $\mu_\parallel = \chi_\parallel = 1.0$, and $\mu_\perp = \chi_\perp = 0.01$. The domain is $|x/\rho_s| < L_x = 40$ and $L_y = 10\pi$. Seven modes ($0 \leqslant m \leqslant 6$) are included in this calculation with $k_y \rho_s = 0.2$ for the $m = 1$ mode.

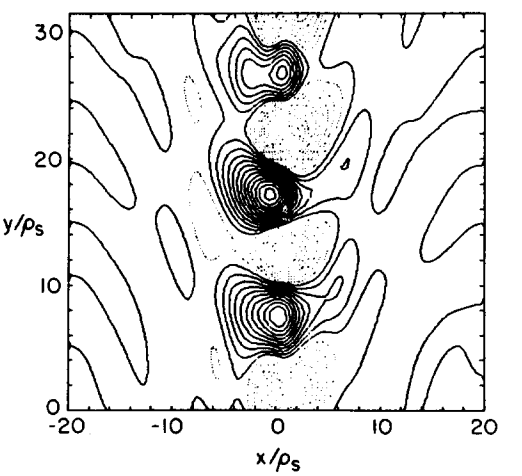

FIG. 9. The contours of constant ϕ at saturation with larger shear $s = 0.5$ obtained from the single-helicity calculation. The other parameters are the same as those used in Figs. 7 and 8, except for $L_x = 20$. The nonlinearly saturated modes are more strongly localized to the mode rational surface at $x/\rho_s = 0$.

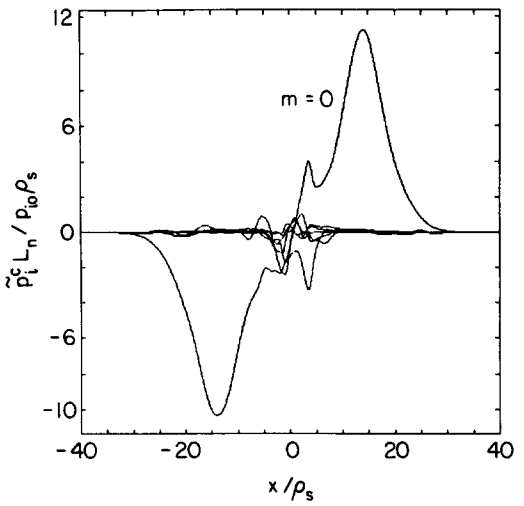

FIG. 10. Fourier cosine components of the perturbed pressure $\tilde{p}_i$ at $\tau = 500$ of the same calculation as Fig. 8. The dominant $m = 0$ (or $k_y = 0$) mode locally cancels the background constant ion pressure gradient K.

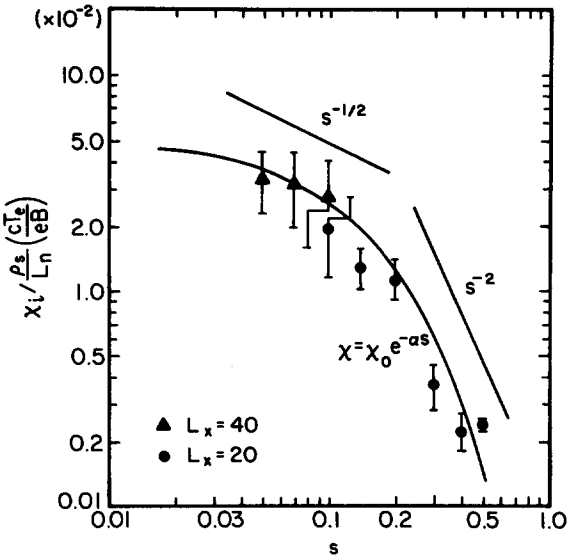

FIG. 11. The anomalous ion heat conductivity χ_i as a function of s, obtained from the single-helicity simulations. The parameters used in the simulations are $K = 3.0$, $\Gamma = 2$, $\mu_\parallel = \chi_\parallel = 1.0$, and $\mu_\perp = \chi_\perp = 0.01$. The domain is $L_x = 40$ for ▲, $L_x = 20$ for ●, and $L_y = 10\pi$ for both. The solid curve indicates the scaling of $\chi_i = \chi_0 \exp(-\alpha s)$ with $\chi_0 = 5.34 \times 10^{-2} \times (\rho_s/L_n)(cT_e/eB)$ and $\alpha = 7.2$. The error bars represent the fluctuation level defined by Eq. (72).

and the space average $\langle\ \rangle$, which is somewhat different from Eq. (10), is defined by

$$\langle\ \rangle = \frac{1}{\Delta L_y L_z} \int_{-L_x}^{L_x} d\tilde{x} \int_0^{L_y} d\tilde{y} \int_0^{L_z} d\tilde{z}, \tag{71}$$

where Δ denotes the mode width in the x direction. In practice, the time average is taken over a reasonably long time period of T after the saturation is attained. The size of the mode width Δ is used as a normalization factor of Eq. (71) so that averaged values calculated from Eq. (70) do not depend on choice of L_x when the modes are localized. In our simulations, the definition of Δ is given as follows: for a function $f(\tilde{x})$ representing a physical quantity averaged over $\tilde{y}$ and $\tilde{z}$, we define

$$I(\tilde{x}) = \begin{cases} 1, & \text{if } |f(\tilde{x})| \geqslant f_{\max}/10, \\ 0, & \text{if } |f(\tilde{x})| < f_{\max}/10, \end{cases}$$

where $f_{\max}$ is the maximum value of $|f(\tilde{x})|$ on $|\tilde{x}| \leqslant L_x$. Then the mode width Δ is defined by

$$\Delta = \int_{-L_x}^{L_x} I(\tilde{x}) d\tilde{x},$$

which gives a reasonable estimate of the "support" of the localized mode. The fluctuation level of the space-averaged anomalous ion heat conductivity $\chi_i(t) = \langle \tilde{p}_i \tilde{v}_{1r} \rangle / (-p_{i0}')$ is then given by

$$\Delta\chi_i = \left\{ \overline{[\chi_i(t) - \chi_i]^2} \right\}^{1/2}, \tag{72}$$

which is shown by error bars in the following figures for χ_i.

The anomalous ion heat conductivity χ_i calculated from Eq. (70) is shown in Fig. 11 as a function of shear. As expected from the linear analysis of Sec. III, the strong shear stabilization of the mode is observed for $s \gtrsim 0.2$, where χ_i decreases approximately as $\chi_i \propto s^{-2}$. On the other hand, χ_i seems to become an independent function of s as s approaches zero, which agrees with the conjecture based on the mixing length theory discussed in Sec. III. In the intermediate range $0.05 \lesssim s \lesssim 0.2$, which is of practical importance for current tokamak experiments, χ_i is a weakly decreasing function of s given by $\chi_i \propto s^{-\beta}$ with $\frac{1}{2} \lesssim \beta \lesssim 2$. The shear dependence of χ_i is found to be well parametrized by $\chi_i = \chi_0 \exp(-\alpha s)$ with $\chi_0 = 5.34 \times 10^{-3} (\rho_s/L_n)(cT_e/eB)$ and $\alpha = 7.2$ for the entire range of s.

Figure 12 shows the anomalous ion heat conductivity χ_i as a function of $K - K_c = (\eta_i - \eta_{ic}) T_i/T_e$, where $K_c = 0.4$. As $K \to K_c$ or the system approaches the marginally stable state, the dependence of χ_i on K is given by $\chi_i \propto (K - K_c)$, which verifies the result of the nonlinear analysis given in Eq. (69). For larger K, χ_i shows a slight deviation from the linear dependence on $K - K_c$. In Figs. 11 and 12 the magnitude of the numerically obtained $\chi_i/(cT_e/eB)(\rho/L_n)$ is, however, significantly small (order of 10^{-2}) and would have a weak effect on the global transport of confined plasmas. This small magnitude χ_0 is due to the quasilinear saturation mechanism which saturates the modes with small amplitude. In confinement experiments, however, the mean ion pressure gradient is maintained constant for a significant period of time in each discharge since the plasma is continuously heated from some external heat sources and cooled at the edge. This situation, which leads to turbulent saturation rather than quasilinear saturation, is simulated in the 3-D calculations presented in the rest of this section. We, however, emphasize the importance of the results of 2-D nonlinear simulations presented above despite their small saturation amplitudes for the following two reasons. First, the results presented here are nonlinear solutions of the system (5)–(7) (together with the boundary conditions given in Sec. II), which is widely used as a simple fluid model of the η_i mode in the literature. We note that this

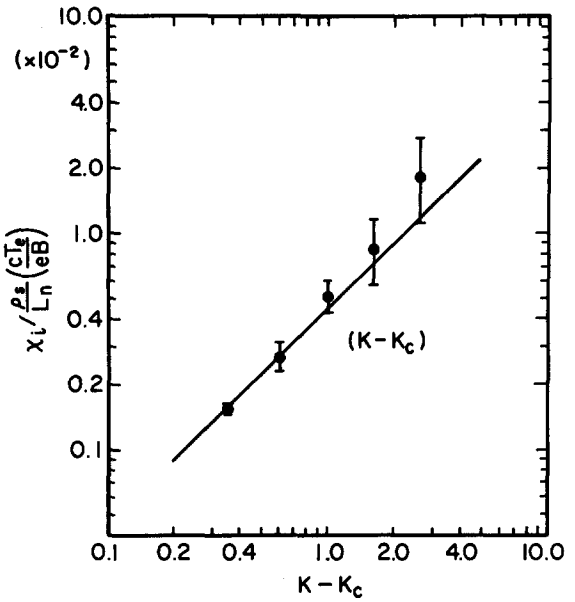

FIG. 12. The anomalous ion heat conductivity χ_i as a function of $K-K_c$, obtained from the single-helicity simulations. The parameters used in the simulations are $s=0.1$, $\Gamma=2$, $\mu_\parallel=\chi_\parallel=1.0$, $\mu_\perp=\chi_\perp=0.1$, and $K_c=0.4$. The domain is given by $L_x=20$ and $L_y=10\pi$. The solid line is the curve proportional to $(K-K_c)$.

system intrinsically saturates the mode quasilinearly. Second, and more important, 2-D solutions of many nonlinear fluid problems often show a qualitative resemblance to their corresponding 3-D (turbulent) solutions. We particularly expect the dependence of χ_i on s and $K-K_c$ shown in Figs. 11 and 12, respectively, to be similar to that of the 3-D turbulent system.

We now proceed to the 3-D simulations. The size of the domain used throughout the following calculations is given by $L_x=20$, $L_y=10\pi$, and $L_z=7.5\pi$, so that the smallest finite wave numbers are $k_y\rho_s=0.2$ and $k_zL_n=0.267$ and the distance between the two rational surfaces of the $m=1/n=0$ mode and the $m=1/n=1$ mode in the case of shear $s=0.1$ is about $13\,\rho_s$. The equally spaced 150 mesh points are used for discretization of the interval $-L_x\leqslant\tilde{x}\leqslant L_x$ and 58–130 modes are chosen for the Fourier representation that cover at least all the unstable modes with $-3\leqslant n\leqslant 3$. In all the 3-D simulations presented in this section, we use the perpendicular diffusion parameters $\mu_\perp=\chi_\perp=0.1$, which are larger than those used in the 2-D simulations presented above. These diffusion coefficients significantly reduce numerical instabilities without requiring higher resolution. It is checked numerically that dependence of saturation levels of turbulence on the diffusion coefficients $\mu_\perp$ and $\chi_\perp$ is weak as long as $\mu_\perp,\chi_\perp\lesssim 0.1$.

To model the confinement experiments without local quasilinear saturation, we add the following auxiliary heat $q=q(x,\tau)$ to Eq. (7), which induce turbulent saturation (or the saturation of modes due to the balance between the free-energy source and high-**k** diffusion) rather than the quasilinear saturation. Equation (7) then becomes

$$\frac{\partial p}{\partial\tau}=-K\frac{\partial\phi}{\partial y}-\Gamma\nabla v-\{\phi,p\}+q+\chi_\perp\nabla_\perp^2p+\chi_\parallel\nabla_\parallel^2p, \tag{73}$$

where

$$q=\langle\{\phi,p\}\rangle_{m=n=0}=\frac{1}{L_yL_z}\int_0^{L_y}d\tilde{y}\int_0^{L_z}d\tilde{z}\{\phi,p\}.$$

It now follows that the $m=n=0$ component $p_{00}=\langle p\rangle_{m=n=0}$ of p satisfies the diffusion equation

$$\frac{\partial p_{00}}{\partial t}=\chi_\perp\nabla_\perp^2p_{00},$$

which leads to $p_{00}=0$ in the steady state. The physical meaning of $q(x)$ is the additional heat which prevents the flattening of the mean ion pressure gradient (i.e., the sum of the constant background ion pressure gradient K and the $m=n=0$ component of the perturbed pressure p) by carrying the thermal energy from the region $\tilde{x}<0$ to the region $\tilde{x}>0$. Our simulations show that, without the heat $q(x,\tau)$, the flattening of the mean ion pressure gradient occurs even in the multihelicity calculations. We note that the energy equation (13) still holds for the system (5), (6), and (73) since

$$\langle pq\rangle=\langle p_{00}q\rangle=0.$$

Introducing q in the pressure equation, therefore, does not introduce any additional free-energy source or sink to the system but simply readjusts the plasma in such a way that the mean ion pressure gradient remains as constant K in the evolution of time. The artificial heat q thus models both the heating mechanism of the core plasma and the cooling mechanism of the edge plasma which maintain a finite mean ion pressure gradient for a significant period of time in a confined plasma. Numerically, adding q to the pressure equation is equivalent to setting $p_{00}=0$ at each time step.

The turbulent saturation of the total energy E_T is shown in Fig. 13 for $K=3$ and $s=0.1$. In this 3-D simulation, 130 modes ($0\leqslant m\leqslant 9$ and $-6\leqslant n\leqslant 6$) are included. Figure 14 shows the time evolution of the perpendicular kinetic energy $E_{\perp m,n}$ of a few sampled (m,n) modes under the same conditions. Here $E_{\perp mn}=\langle|\nabla_\perp\phi_{mn}(\tilde{x},\tilde{y},\tilde{z},\tau)|^2\rangle$ with

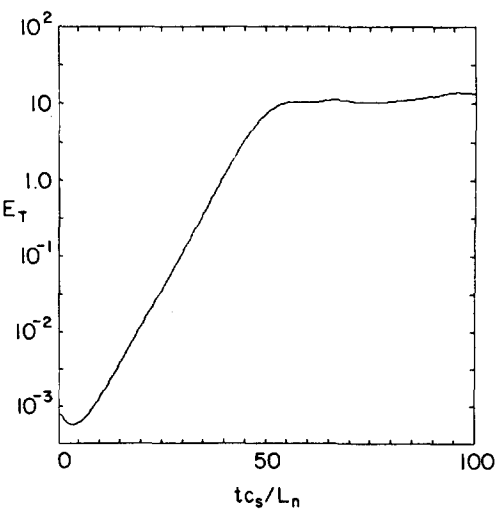

FIG. 13. Time evolution of the total energy $E_\perp$ obtained from the 3-D calculation with 130 modes ($0<m<9$ and $-6<n<6$). The parameters used here are $K=3.0$, $s=0.1$, $\Gamma=2$, $\mu_\parallel=\chi_\parallel=1.0$, and $\mu_\perp=\chi_\perp=0.1$. The turbulent saturation is observed at $\tau=tc_s/L_n\simeq 50$.

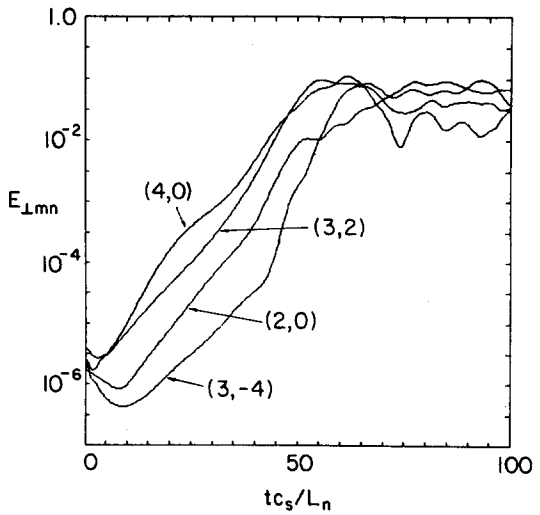

FIG. 14. Time evolutions of the perpendicular kinetic energy $E_{\perp mn}$ of four sampled (m,n) modes are plotted under the same conditions as in Fig. 13. In this case, the $m=4$ modes are linearly most unstable. However, after saturation, the modes with $m\leqslant 3$ reach energy levels similar to those of the $m=4$ modes.

$$\phi_{mn}(\tilde{x},\tilde{y},\tilde{z},\tau)=\phi^{c}_{mn}(\tilde{x},\tau)\cos\psi_{mn}+\phi^{s}_{mn}(\tilde{x},\tau)\sin\psi_{mn}$$

and

$$\psi_{mn}=2\pi(m\tilde{y}/L_y-n\tilde{z}/L_z).$$

In this case, the $m=4$ modes are the linearly most unstable. However, after saturation, the other modes with $m\leqslant 4$ also reach the energy levels similar to that of the $m=4$ modes. Integrating the perpendicular kinetic energy in $\tilde{z}$ or $E_{\perp m}=\Sigma_n E_{\perp mn}$ we show in Fig. 15 the perpendicular kinetic energy spectrum obtained by time averaging $\Sigma_n E_{\perp mn}$, over $60\leqslant tc_s/L_n\leqslant 100$. It is shown that the $m=3$ mode $(k_y\rho_s=0.6)$ has the peak and the other modes with $m\leqslant 4$ also have relatively high energy levels. The modes with $m\geqslant 5$ or $k_y\rho_s\geqslant 1.0$ decay significantly.

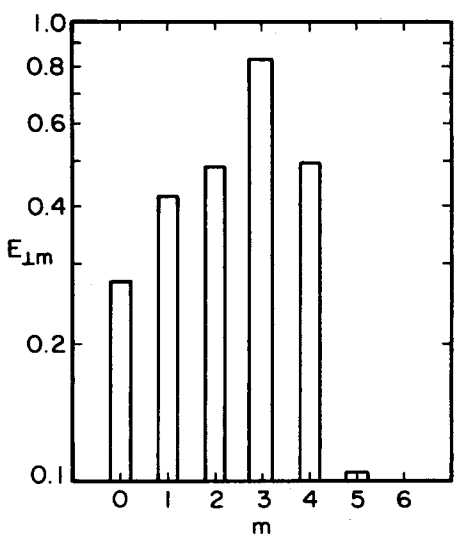

FIG. 15. The perpendicular kinetic energy spectrum $E_{\perp m}$ obtained from the time average of $\Sigma_n E_{\perp mn}$ over $60\leqslant tc_s/L_n\leqslant 100$ under the same conditions as in Fig. 13. The modes with $m\leqslant 4$ have relatively high energy levels with the peak at $m=3$ (or $k_y\rho_s=0.6$) while the modes with $m\geqslant 5$ are significantly weaker.

The potential contours at saturation are shown in Figs. 16(a) and 16(b). There are three rational surfaces for the $m=1$ modes (and more rational surfaces for higher m modes) in the domain of Fig. 16(a), where $s=0.1$, with one being at $x/\rho_s=0$ and each being separated by distance about $13\rho_s$. Some convection cells are, however, widespread from the rational surfaces, indicating that strong nonlinear interaction is taking place. For comparison, the potential contours of zero shear are shown in Fig. 16(b).

The dependence of the anomalous ion heat conductivity χ_i on the shear s obtained from the 3-D simulations is shown in Fig. 17 for $K=3.0$, where χ_i scales as $\chi_i=\chi_0\exp(-\alpha s)$ with $\chi_0=1.58(\rho_s/L_n)(cT_e/eB)$ and $\alpha=3.7$. The peak of χ_i as a function of s is obtained at $s=0$ as expected from the mixing length estimates (Sec. III) and from the 2-D simulations. In the 3-D simulations, however, the magnitude of χ_i is significantly larger than that of the quasilinearly saturated single helicity modes shown in Fig. 11. Figure 18 shows the dependence of χ_i on $K-K_c=(\eta_i-\eta_c)T_i/T_e$, obtained from the 3-D simulations for $s=0.1$ and $K_c=1.3$. As in the case of Fig. 12, χ_i is almost linear in $(K-K_c)$ although the χ_i deviates from the linear dependence when $K-K_c$ is small. This is due to transition or successive bifurcation[21] from the coherent nonlinear modes near the marginally stable state $(K\simeq K_c)$ to turbulence $(K-K_c\gg K_c)$.

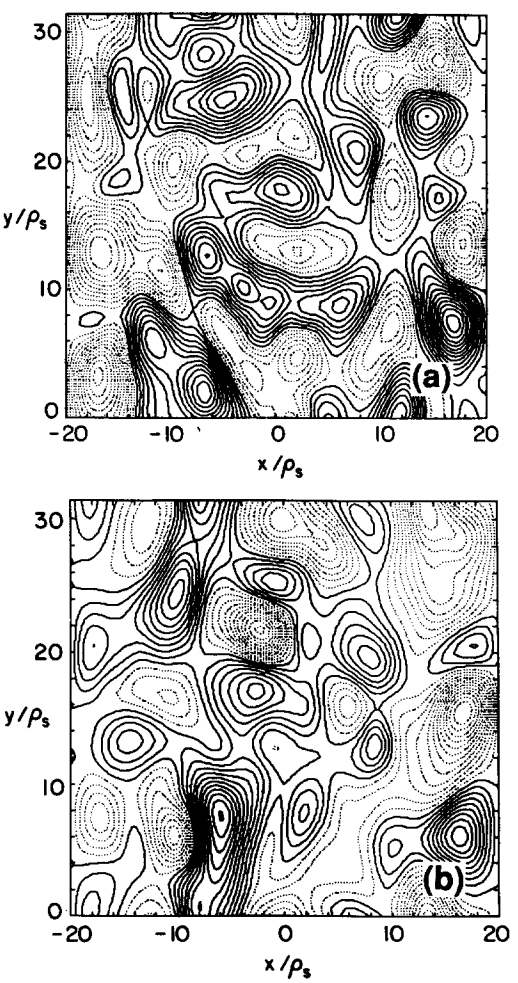

FIG. 16. The contours of constant ϕ at saturation. (a) The case of $s=0.1$, obtained from the simulation shown in Fig. 13 at $\tau=100$. (b) The case of $s=0$, where all the other parameters are the same as those used in the simulation of Fig. 13.

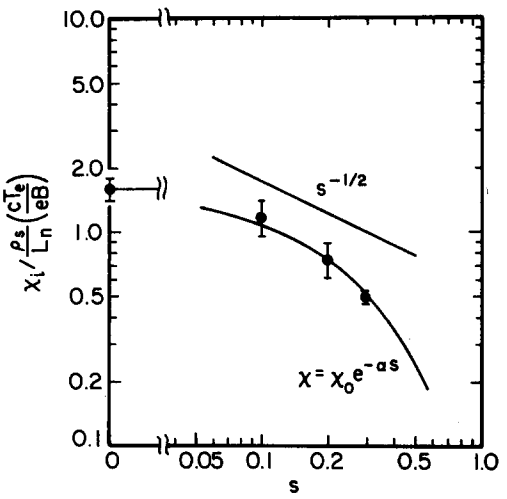

FIG. 17. The anomalous ion heat conductivity χ_i as a function of s, obtained from the 3-D simulations. The parameters used in the simulations are $K=3.0$, $\Gamma=2$, $\mu_{\parallel}=\chi_{\parallel}=1.0$, and $\mu_{\perp}=\chi_{\perp}=0.1$. The domain is $L_x=20$, $L_y=10\pi$, and $L_z=7.5\pi$. The solid curve indicates the scaling of $\chi_i=\chi_0\exp(-\alpha s)$ with $\chi_0=1.58(\rho_s/L_n)(cT_e/eB)$ and $\alpha=3.7$.

In the 2-D simulations with finite magnetic shear, all the modes are localized at the single rational surface $\tilde{x}=0$ and fall significantly within the boundaries. Therefore, the boundary conditions do not affect saturation levels of the modes in the 2-D simulations. However, in the 3-D simulations on a finite-size domain, the boundary conditions may affect saturation levels of turbulence by reflecting drift waves at the boundaries $|\tilde{x}|=L_x$ since some of the rational surfaces of strongly excited modes may be close to the boundaries. In the 3-D simulations presented in this work, however, we did not make any particular effort to avoid the boundary effects on saturation levels of turbulence. Instead, when we survey parameters, we vary only one parameter and fix all the other parameters including the size of the domain. In other words, we regard the problem as the one to be solved on a fixed finite domain with the given boundary conditions, assuming that the size of the domain is large enough so that this slab model represents some of the important features of toroidally confined plasmas.

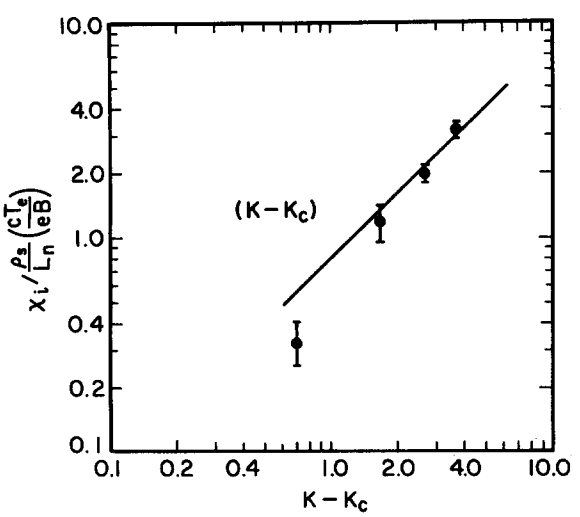

FIG. 18. The anomalous ion heat conductivity χ_i as a function of $K-K_c$, obtained from the 3-D simulations. The parameters used in the simulations are $s=0.1$, $\Gamma=2$, $\mu_{\parallel}=\chi_{\parallel}=1.0$, $\mu_{\perp}=\chi_{\perp}=0.1$, and $K_c=1.3$. The domain is the same as in Fig. 17. The solid line is the curve proportional to $(K-K_c)$.

In this point of view, throughout the 3-D simulations presented here, we fix both the box size $2L_x\times L_y\times L_z=40\times 10\pi\times 7.5\pi$ and the number of the rational surfaces for the $m=1$ modes included in the calculations, i.e., $-3\leqslant n\leqslant 3$. Therefore, when shear is large ($s\gtrsim 0.2$), all the strongly excited modes fall within boundaries and the boundary effect is ignorable, whereas, when shear is weak ($0\leqslant s\lesssim 0.1$), some of the rational surfaces of the strongly excited modes lie outside the domain. We therefore examined the boundary effects in the cases of weak shear by varying L_x in numerical calculations.

The study of varying L_x at small shear showed that although the modes near the boundaries tends to be enhanced by reflection, the magnitude of enhancement of the anomalous heat transport χ_i is not significant, as long as the parameter space we examined in this work is concerned. For example, as shown in Fig. 17, $\chi_i\simeq 1.2(\rho_s/L_n)(cT_e/eB)$ when $s=0.1$, $K=3.0$, and $L_x=20$. If we increase L_x to $L_x=50$ with all the other parameters unchanged, reflection of the modes at the boundaries is eliminated and the anomalous heat transport decreases to $\chi_i=0.9(\rho_s/L_n)(cT_e/eB)$ or about 25% decrease from the value at $L_x=20$.

Summarizing the analyses in Secs. III and IV and the numerical results in this section, we obtain the scaling of the anomalous ion heat transport given by

$$\chi_i=g\frac{\rho_s}{L_n}\left(\frac{cT_e}{eB}\right)(K-K_c)\exp(-\alpha s)$$

$$=g\frac{\rho_s}{L_n}\left(\frac{cT_i}{eB}\right)(\eta_i-\eta_{ic})\exp(-\alpha s). \qquad (74)$$

As suggested by the mixing length formula [Eq. (50)], the numerical simulations shown in Figs. 11 and 17, and the numerical results in Ref. 7, χ_i seems to scale as $\chi_i\propto s^{-1/2}$ near $s=0.1$. Taking this into account, we obtain $\alpha\simeq 5$ since $e^{-5s}\simeq 0.2s^{-1/2}$ near $s=0.1$ although numerically obtained α varies as $3\lesssim\alpha\lesssim 7$. From the magnitudes of χ_i presented in Figs. 17 [where $K-K_c\simeq 1.7$ and $K_c=1.3$ is a weak function of shear as shown in Eq. (41)] and 18, the constant g is of order unity when turbulent saturation occurs. Equation (74) with $g\simeq 1$ and $\alpha\simeq 5$ thus gives the scaling of χ_i in a practically useful range of the parameter space for fusion-plasma confinement studies.

VI. DISCUSSION AND CONCLUSIONS

We have analyzed the nonlinear ion temperature gradient driven mode, or η_i mode, of the sheared slab model based on rigorous analyses and numerical simulations of the reduced fluid Eqs. (5)–(7). A new formula for the anomalous ion heat conductivity due to the η_i-mode turbulence is derived, which differs significantly from some of the previously reported results.[8–10] It is found from the linear analysis that the finite magnetic shear s has the stabilizing effect reducing the growth rate of the fastest growing linear η_i mode. Consequently, the fluctuation levels and the associated anomalous

ion heat conductivity χ_i are decreasing functions of the shear s.

It is also shown with the use of the amplitude expansion method[21] that χ_i depends on $(\eta_i - \eta_{i,c})$ linearly near the marginally stable state. This dependence of χ_i on $(\eta_i - \eta_{i,c})$ is also obtained numerically in fully developed turbulent states. Numerical simulations demonstrate the turbulent saturation of the η_i mode, as well as the quasilinear saturation under certain conditions. A good parametrization summarizing the analytic and numerical results for the anomalous ion heat conductivity $\chi_i(s,\eta_i)$ is given by

$$\chi_i = g\left(\frac{\rho_s}{L_n}\right)\left(\frac{cT_i}{eB}\right)(\eta_i - \eta_{i,c})\exp(-\alpha s), \tag{75}$$

where $\alpha \simeq 5$ and $g \simeq 1$. For typical plasma parameters of the TFTR supershot[3] at the half-minor radius, the formula (75) gives $\chi_i = 5.1\ \mathrm{m^2/sec}$, where $T_i = 10$ keV, $B = 4.6$ T, $\rho_s = 1.2\times 10^{-3}$ m, $L_n = 0.52$ m, $\eta_i = 2.7$, $\eta_{i,c} = 1$, and $s = 0.1$ are used. This gives a comparable magnitude of the ion heat conductivity measured in the experiments.[3]

The parameter α used in Eq. (75) is generally a function of $K = (1+\eta_i)T_i/T_e$. Since we are concerned with a parameter range of $\eta_{i,c} \leqslant \eta_i \lesssim 3$, it is practically accurate to use a constant value $\alpha(K = K_c) \simeq 5$ for α. However, we note that the η_i dependence of α becomes important when $K \gg 1$. In particular, when $K \to \infty$, the scaling of χ_i is given by

$$\chi_i = g\frac{\rho_s}{L_T}\left(\frac{cT_i}{eB}\right)\exp\left(-\beta\frac{s}{K}\right),$$

where $\beta \simeq 4$ and $s/K \to (T_e/T_i)(L_T/L_s)$. In other words, $\alpha(K) \to \beta/K$ as $K \to \infty$. Derivation of this χ_i scaling and the dependence of α on general K will be discussed in the future.

Horton, Estes, and Biskamp obtained[7]

$$\chi_i = g\frac{\rho_s}{L_n}\left(\frac{cT_i}{eB}\right)\frac{(1+\eta_i)^{1/2+\epsilon}}{s^{1/2}}, \tag{76}$$

basically from numerical simulations of the system (5)–(7) giving $g \simeq 0.3$ and $|\epsilon| \lesssim 0.5$. The numerical code used in Ref. 7 employs a finite difference method in x,y, and z with upwind derivatives in the $\mathbf{E}\times\mathbf{B}$ convection, which is a different algorithm from the one used in the present work. Considering the fact that $e^{-5s} \simeq 0.2 s^{-1/2}$ numerically near $s = 0.1$ and taking $\epsilon = 0.5$, the χ_i scaling of Eq. (76) is somewhat similar to Eq. (75). However, the scaling of Eq. (75) obtained in the present work represents χ_i under a much wider range of the shear parameter s. We also note that the χ_i scaling of Eq. (75) has an explicit dependence on the critical ion temperature gradient $\eta_{i,c}$ that is missed by the incompressible theory formulas varying as $(1+\eta_i)^{\beta}$.

Some of the previously reported scalings of the anomalous ion heat conductivity[8-10] χ_i significantly differ from Eq. (75), although they are reported to be based on the same system of Eqs. (5)–(7). The main difference between these previously reported scaling and Eq. (75) is the shear dependence of χ_i: In Refs. 8 and 9, χ_i is asserted to be an increasing function of the shear s and χ_i vanishes as $s \to 0$. Also the scalings of χ_i derived in those references have a different dependence on $K = (1+\eta_i)T_i/T_e$. In order to clarify what leads to this contradiction between the previously reported results and the newly obtained result, we present here brief critiques of Refs. 8–10.

A. Critiques of earlier theories

The difference between the results of Refs. 8–10, and from Eq. (75) essentially originates from the inconsistent treatment of the linear properties of the η_i mode in Refs. 8–10, not from the nonlinear analyses. The problem arises either from oversimplification of the nonlinear system that leads to a system having qualitatively different linear properties or from the *ad hoc* choice of "typical" linear properties on which the nonlinear analyses of the mode is based. To make this point clearer, we here repeat three important linear properties of the η_i mode in Eqs. (5)–(7), which seem not to be given sufficient attention in the previous works.

(i) The fastest growing linear mode occurs when the wave number is chosen in such a way that the drift wave source term $(1 + K\nabla_\perp^2)$ in the right-hand side of Eq. (5) [or the second term in the left-hand side of Eq. (14)] becomes small, i.e., $k_y\rho_s \simeq K^{-1/2}$. Since the case where $K = (1+\eta_i)\times T_i/T_e = O(1)$ is of most interest, it is important to realize that as long as the system (5)–(7) is concerned, the modes with $k_y\rho_s = O(1)$ play an important role in the nonlinear system. In reality, the dynamics of such modes may be modified by kinetic effects[6,25,26] to some extent, but this is another question.

(ii) The largest growth rate γ of the η_i spectrum is a *decreasing* function of the magnetic shear s and γ approaches its maximum value as $s \to 0$, although the shear dependence of γ is weak when $s \ll 1$. This shear dependence is because the radial eigenmode number l that gives the largest growth rate increases as s decreases, so as to keep $\tilde{s} = (2l+1)s$ approximately constant. It may, therefore, be misleading to state that the shear dependence of the growth rate $\mathrm{Im}\,\Omega$ is given by $\mathrm{Im}\,\Omega \propto (2l+1)sK$ when $k_y^2\rho_s^2K \ll 1$ and by $\mathrm{Im}\,\Omega \propto \sqrt{(2l+1)sK}$ when $k_y^2\rho_s^2K \simeq 1$. We must understand that the radial mode number l giving the largest growth rate is also a function of the shear s.

(iii) There is a shear stabilization effect reducing the linear growth rate for larger shear $s \gtrsim 0.1$. This stabilization effect is due to the compression of the parallel velocity field and to parallel diffusion.

Keeping these linear properties of the η_i mode in mind, we proceed to critiques of the previous works.

1. The work of Connor (Ref. 8)

Connor derived the formula of the anomalous heat conductivity

$$\chi_i = g(\rho_s/L_n)(cT_e/eB)K^{3/2}s \tag{77}$$

in the limit of $sK \ll 1$ [Eq. (44) in Ref. 8], where g is a constant. In deriving Eq. (77), the following terms are dropped from the system (5)–(7) as ignorable: the parallel compression $\Gamma_p\nabla_\parallel v$, the inertia of the vorticity $(1-\nabla_\perp^2)\partial\phi/\partial\tau$ and the parallel electric field $-\nabla_\parallel\phi$. No diffusion terms are included either, which we do not question, however, at this point since it is generally considered that turbulence has a weak dependence on the diffusion coefficients. Inclusion of

the nonlinearity due to the finite Larmor radius effect or $\{p,\nabla_\perp^2\phi\}+\{\partial p/\partial x,\partial\phi/\partial x\}+\{\partial p/\partial y,\partial\phi/\partial y\}$ in the vorticity equation [Eq. (35) of Ref. 8] does not change the argument presented here. Dropping the parallel compression $\Gamma_p\nabla_\parallel v$, the inertia of the vorticity due to the polarization drift $-\nabla_\perp\partial\phi/\partial\tau$ and the parallel electric field $-\nabla_\parallel\phi$ causes, in fact, less significant problems.

After ignoring these three linear terms from the system (5)–(7), the linear eigenvalue is now given by the following quadratic equation

$$\Omega^2-(1-\tilde{k}^2K)\Omega+iK\tilde{s}=0, \tag{78}$$

where $\tilde{s}=(2l+1)s$. We note that Im Ω obtained from this equation becomes ∞ as $\tilde{s}=(2l+1)s\to\infty$, unlike the case of Eq. (20). This suggests that the fastest growing mode of this simplified system has the infinite linear growth rate with $l=\infty$ and the initial boundary-value problem of this system is mathematically ill-posed. We, however, do not worry about this point here either, assuming that such high-radial eigenmodes be damped in reality by some perpendicular diffusion that is not explicitly included in the system of Ref. 8. In addition to these assumptions, however, Connor assumed that the inertia $\partial\phi/\partial\tau$ of Eq. (5) be dropped, which is crucial to obtain the explicit form of χ_i given by Eq. (77). This assumption is equivalent to ignoring the first term of Eq. (78) and the linear growth rate is now given by

$$\Omega=i\tilde{s}K/(1-\tilde{k}^2K). \tag{79}$$

It is clear that as $\tilde{k}^2=k_y^2\rho_s^2\to 1/K$, the linear growth rate approaches ∞ while the coefficient of the second term of Eq. (78) approaches 0. It follows that dropping the first term of Eq. (78) or dropping the inertia $\partial\phi/\partial\tau$ from Eq. (5) may not be justified when $\tilde{k}^2\simeq 1/K$. In fact, eliminating the first term Ω^2 of Eq. (78) prevents the thermal mode from being excited, which is the main mechanism of the η_i mode, as discussed in Sec. III. Although nonlinearly saturated states may not be fully explained by these linear properties, we believe that the assumption made in Ref. 8 leads to oversimplification of the original nonlinear system, since this simplified system no longer possesses the qualitatively correct linear properties of the η_i mode. The correct linear properties near the maximum growth rate may be essential in maintaining correct form of the turbulence against the dissipation. We also note that our nonlinear numerical simulations suggest that the time derivatives of ϕ, p, and v are of the same order.

2. The work of Lee and Diamond (Ref. 9)

In Ref. 9, Lee and Diamond derive from the system (5)–(7)

$$\chi_i=g(\rho_s/L_n)(cT_e/eB)K^2s(k_y\rho_s)_{\rm rms}, \tag{80}$$

where $(k_y\rho_s)_{\rm rms}\simeq 0.4$ and g is a weak function of η_i. The essence of this work is well represented in subsection A, "Heuristic description," of Sec. III of Ref. 9. In this subsection, based on the so-called one-point renormalized equation, they derived the following two relations [Eqs. (36) and (38) in Ref. 9]:

$$D_k\simeq K^{1/2}k_\parallel'\Delta_k^3,$$

$$\Delta_k\simeq(D_k/k_\parallel')^{1/4}$$

by balancing certain key terms of the system. Here D_k is the k-dependent anomalous diffusion coefficient arising from the nonlinearity $\{\phi,p\}$, or the $\mathbf{E}\times\mathbf{B}$ convection of the pressure fluctuation, Δ_k is the k-dependent radial correlation length, and $k_\parallel'=k_y/L_s$. These relations lead to the decorrelation rate $\Delta\omega_k$ ($=D_k/\Delta_k^2$) associated with $\mathbf{E}\times\mathbf{B}$ turbulent convection and the radial correlation length Δ_k given by

$$\Delta\omega_k\propto sK, \tag{81}$$

$$\Delta_k\simeq\sqrt{K}, \tag{82}$$

which basically corresponds to the choice made to derive Eq. (47) in Sec. III. This balancing of certain linear terms of the system is essentially equivalent to the approximation that Connor made in Ref. 8, leading to the linear growth rate of Eq. (79) with the extra assumption $\tilde{k}^2K\ll 1$, i.e.,

$$\Omega\simeq isK. \tag{83}$$

Thus, it is not just a coincidence that the shear dependence of χ_i given in Refs. 8 and 9 are the same. Since the one-point renormalized equations, in which all the nonlinear convection terms are simply replaced by linear diffusion terms with diffusion coefficients to be determined, give a linear system, one must use the linear properties of the system one way or another at some point if he wishes to evaluate fluctuation levels and anomalous transport coefficients from the one-point renormalized equations. In this sense, it is not clarified nor justified in Ref. 9 why these authors choose the particular way of balancing the terms that lead to the linear growth rate of Eq. (83) [which was subsequently used as the decorrelation rate $\Delta\omega_k$ of Eq. (81)] and rule out the possibility of balancing different terms in such a way that a larger growth rate Im $\Omega\propto\sqrt{sK}$ with $k^2\rho_s^2\simeq 1/K$ is obtained. Although it is observed in numerical simulations that the modes with smaller $k_y\rho_s$ have larger amplitude in the turbulent state, these modes are produced by nonlinear interactions of higher-k_y primary modes and not by the strong linear instability. In fact, these nonlinearly excited low-k_y modes have different mode properties from the linearly excited low-k_y modes. Therefore, detailed justification is needed if one attempts to associate the properties given in Eqs. (81) and (82) of the long-wavelength linear eigenmodes ($k^2K\ll 1$) with the nonlinearly excited low-k_y modes. We also note that Lee and Diamond relate the pressure fluctuation $\tilde{p}_k$ to the electrostatic potential fluctuation $\tilde{\phi}_k$ as

$$\tilde{p}_k\simeq iK\omega_{*e}\tilde{\phi}_k/\Delta\omega_k \tag{84}$$

[Eq. (35) of Ref. 9] by balancing the anomalous diffusion term to the ion temperature gradient driven term in their one-point renormalized equations. Using the relation, Eq. (84), is, in fact, crucial to obtain an explicit form of the anomalous diffusion coefficients from their two-point renormalization technique presented in subsection B of Sec. III of Ref. 9. Despite their elaboration of the two-point renormalization technique, therefore, the final results derived therein [such as Eq. (85) and Eq. (92) of Ref. 9] heavily depend on the choice of the unjustified linearlike relation Eq. (84) taken from the *one-point* equations. This approximation makes

obscure the accuracy of the conclusions of the two-point renormalization technique in Ref. 9.

3. The work of Terry et al. (Ref. 10)

Terry *et al.* derive the anomalous diffusion coefficient given by

$$D_k \simeq \omega_* \rho_s^2 (2l+1)^2 K^2 s \tag{85}$$

[Eq. (10) of Ref. 10] to the lowest order of s, from the system (5)–(7), using the mixing length estimate and the one-point renormalization technique. It is claimed that the larger radial eigenmode number $l(1 \leqslant l \lesssim 10)$ significantly increases D_k over the D_k obtained by Lee and Diamond in Ref. 9 as the higher-order radial eigenmodes are more strongly excited and bear a broader mode structure. Since the method used to obtain the scaling of Eq. (85) is similar to that of Ref. 9, the critique of Ref. 9 presented above also applies to Ref. 10. In addition, it seems inconsistent that the authors of Ref. 10 attempt to maximize the growth rate by varying only the radial mode number l while keeping k_y (or the poloidal mode number m) small, i.e., $k_y^2 \rho_s^2 K \ll 1$.

These critiques and the fact that none of these previous works[8–10] provide nonlinear simulations supporting their results indicate that these previously reported χ_i scalings are not justified. Given the more rigorous analyses and direct numerical simulations of the system (5)–(7) presented in the present work, therefore, we conclude that in the parameter range $sK \lesssim 1$ of interest, the χ_i scalings reported in Refs. 8–10 are erroneous and that the correct scaling of χ_i due to the η_i-mode turbulence in a sheared slab geometry is given by Eq. (75). Other properties of the η_i mode in tokamaks due to toroidicity and kinetic effects are, of course, beyond the scope of the present work.

ACKNOWLEDGMENTS

The authors wish to thank B. G. Hong, M. Wakatani, N. Nakajima, K. C. Shaing, J. P. Mondt, G. W. Hammett, and J. W. Connor for valuable discussions. We are also grateful to M. N. Rosenbluth for helpful comments on the original manuscript.

The work was supported by U. S. Department of Energy Contract No. DE-FG05-80ET-53088.

[1] M. Greenwald, D. Q. Winn, S. Milora, R. Parker, and S. Wolfe, Phys. Rev. Lett. **53**, 352 (1984).
[2] F. X. Sölder, E. R. Müller, F. Wagner, H. S. Bosch, A. Eberhagen, H. U. Fahrbach, G. Fussmann, O. Gehre, K. Gentle, J. Gernhardt, O. Gruber, W. Herrmann, G. Janeschitz, M. Kornherr, K. Krieger, H. M. Mayer, K. McCormick, H. D. Murmann, J. Neuhauser, R. Nolte, W. Poschenrieder, H. Röhr, K.-H. Steuer, U. Stroth, N. Tsois, and H. Verbeek, Phys. Rev. Lett. **61**, 1105 (1988).
[3] R. J. Fonck, R. Howell, K. Jaehnig, L. Roquemore, G. Schilling, S. Scott, M. C. Zarnstorff, C. Bush, R. Goldston, H. Hsuan, D. Johnson, A. Ramsey, J. Schivell, and H. Towner, Phys. Rev. Lett. **63**, 520 (1989).
[4] D. L. Brower, W. A. Peebles, S. K. Kim, N. C. Luhmann, W. M. Tang, and P. E. Phillips, Phys. Rev. Lett. **59**, 48 (1987).
[5] L.I. Rudakov and R. Z. Sagdeev, Dokl. Akad. Nauk. SSSR **138**, 581 (1961) [Sov. Phys. Dokl. **6**, 415 (1961)].
[6] B. Coppi, M. N. Rosenbluth, and R. Z. Sagdeev, Phys. Fluids **10**, 582 (1967).
[7] W. Horton, R. D. Estes, and D. Biskamp, Plasma Phys. **22**, 663 (1980).
[8] J. W. Connor, Nucl. Fusion **26**, 193 (1986).
[9] G. S. Lee and P. H. Diamond, Phys. Fluids **29**, 3291 (1986).
[10] P. W. Terry, J.-N. Leboeuf, P. H. Diamond, D. R. Thayer, J. E. Sedlak, and G. S. Lee, Phys. Fluids **31**, 2920 (1988).
[11] To be precise, there are slight differences (such as the diffusion terms taken into account) between the systems used in Refs. 7–10. However, it is easy to show that these differences do not account for the different scalings of χ_i stated in the text.
[12] W. Horton, D.-I. Choi, and W. M. Tang, Phys. Fluids **24**, 1077 (1981).
[13] F. Romanelli, W. M. Tang, and R. B. White, Nucl. Fusion **26**, 1515 (1986).
[14] F. Romanelli, Phys. Fluids B **1**, 1018 (1989).
[15] P. N. Guzdar, L. Chen, W. M. Tang, and P.H. Rutherford, Phys. Fluids **26**, 673 (1983).
[16] R. R. Dominguez and R. E. Waltz, Nucl. Fusion **27**, 65 (1987).
[17] B.-G. Hong and W. Horton, Plasma Phys. Controlled Fusion **31**, 1291 (1989).
[18] S. I. Braginskii, in *Review of Plasma Physics*, edited by M. A. Leontovich (Consultants Bureau, New York, 1965), Vol. 1, p. 205.
[19] W. M. Tang, G. Rewoldt, and L. Chen, Phys. Fluids **29**, 3715 (1986).
[20] T. S. Hahm and W. M. Tang, Phys. Fluids B **1**, 1185 (1989).
[21] S. Hamaguchi, Phys. Fluids B **1**, 1416 (1989).
[22] D. D. Joseph, *Stability of Fluid Motion* (Springer, New York, 1976), Vols. I and II.
[23] W. Park, D. A. Monticello, R. B. White, and A. M. M. Todd, Bull. Am. Phys. Soc. **23**, 779 (1978).
[24] H. R. Strauss, W. Park, D. A. Monticello, R. B. White, S. C. Jardin, M. S. Chance, A. M. M. Todd, and A. H. Glasser, Nucl. Fusion **20**, 628 (1980).
[25] R. E. Waltz, W. Pfeiffer, and R. R. Dominguez, Nucl. Fusion **20**, 43 (1980).
[26] J. Q. Dong, P. N. Guzdar, and Y. C. Lee, Phys. Fluids **30**, 2694 (1987).